

Elastic theory of low-dimensional continua and its applications in bio- and nano-structures

Z. C. Tu^{1,2,*} and Z. C. Ou-Yang^{3,†}

¹*Department of Physics, Beijing Normal University, Beijing 100875, China*

²*II. Institut für Theoretische Physik, Universität Stuttgart, Pfaffenwaldring 57, 70550 Stuttgart, Germany*

³*Institute of Theoretical Physics, Chinese Academy of Sciences, Beijing 100080, China*

This review presents the elastic theory of low-dimensional (one- and two-dimensional) continua and its applications in bio- and nano-structures.

First, the curve and surface theory, as the geometric representation of the low-dimensional continua, is briefly described through Cartan moving frame method. The elastic theory of Kirchhoff rod, Helfrich rod, bending-soften rod, fluid membrane, and solid shell is revisited. The free energy density of the continua, is constructed on the basis of the symmetry argument. The fundamental equations can be derived from two kinds of viewpoints: the bottom-up and the top-down standpoints. In the former case, the force and moment balance equations are obtained from Newton's laws and then some constitute relations are complemented in terms of the free energy density. In the latter case, the fundamental equations are derived directly from the variation of the free energy. Although the fundamental equations have different forms obtained from these two viewpoints, several examples reveal that they are, in fact, equivalent to each other.

Secondly, the application and availability of the elastic theory of low-dimensional continua in bio-structures, including short DNA rings, lipid membranes, and cell membranes, are discussed. The kink stability of short DNA rings is addressed by using the theory of Kirchhoff rod, Helfrich rod, and bending-soften rod. The lipid membranes obey the theory of fluid membrane. The shape equation and the stability of closed lipid vesicles, the shape equation and boundary conditions of open lipid vesicles with free edges as well as vesicles with lipid domains, and the adhesions between a vesicle and a substrate or another vesicle are fully investigated. A cell membrane is simplified as a composite shell of lipid bilayer and membrane skeleton, which is a little similar to the solid shell. The equations to describe the in-plane strains and shapes of cell membranes are obtained. It is found that the membrane skeleton enhances highly the mechanical stability of cell membranes.

Thirdly, the application and availability of the elastic theory of low-dimensional continua in nano-structures, including graphene and carbon nanotubes, are discussed. A revised Lenosky lattice model is proposed based on the local density approximation. Its continuum form up to the second order terms of curvatures and strains is the same as the free energy of 2D solid shells. The intrinsic roughening of graphene and several typical mechanical properties of carbon nanotubes are revisited and investigated based on this continuum form. It is possible to avoid introducing the controversial concepts, the Young's modulus and thickness of graphene and single-walled carbon nanotubes, with this continuum form.

Keywords: Elastic Theory, DNA Ring, Biomembrane, Graphene, Carbon nanotube, Moving frame method

I. INTRODUCTION

We human beings live in a three-dimensional (3D) space which contains many geometric entities composed of atoms or molecules. The length scale of objects observed with our naked eyes is much larger than the distance between nearest neighbor atoms or molecules in the objects. As a result, the objects can be regarded as continua. If one dimension of an object is much larger than the other two dimensions, such as a rod, we call it a one-dimensional (1D) entity. If one dimension of an object is much smaller than the other two dimensions, such as a thin film, we call it a two-dimensional (2D) entity. In this review, the term "low-dimensional continua" represents 1D and 2D entities.

Elasticity is a property of materials. It means that materials deform under external forces, but return to their original shapes when the forces are removed. Elastic theory, the study on the elasticity of continuum materials, has a long history^{1,2} which records

many geniuses such as Hooke (1635–1703), Bernoulli (1700–1782), Euler (1707–1783), Lagrange (1736–1813), Young (1773–1829), Poisson (1781–1840), Navier (1785–1836), Cauchy (1789–1857), Green (1793–1841), Lamé (1795–1870), Saint-Venant (1797–1886), Stokes (1819–1903), Kirchhoff (1824–1887), and so on. Now elastic theory has been a mature branch of physics and summarized in several excellent textbooks.^{2,3,4} Although the classical elastic theory is applied to macroscopic continuum materials, more and more facts reveal that it can be also available for bio- or nano-structures such as short DNA rings,^{5,6,7,8,9,10,11,12,13} α -helical coiled coils,¹⁴ chiral filaments,^{15,16,17,18,19,20,21} climbing plants,^{22,23} bacterial flagella,²⁴ viral shells,^{25,26,27} bio-membranes,^{28,29,30,31,32,33,34,35,36} zinc oxide nanoribbons,^{37,38,39} and carbon nanotubes,^{40,41,42,43,44,45,46} to some extent.

This review presents the elastic theory of low-dimensional continua and its applications in bio- and nano-structures, which is organized as follows: In Sec. II,

we briefly introduce the geometric representation and the elastic theory of low-dimensional continua including 1D rod and 2D fluid membrane or solid shell. The free energy density of the continua is constructed on the basis of the symmetry argument. The fundamental equations can be derived from the bottom-up and the top-down viewpoints. Although they have different forms obtained from these two standpoints, several examples reveal that they are, in fact, equivalent to each other. In Sec. III, the application and availability of the elastic theory of low-dimensional continua in bio-structures, including short DNA rings, lipid membranes, and cell membranes, are discussed. We investigate the kink stability of short DNA rings, the elasticity of lipid membranes, and the adhesions between a vesicle and a substrate or another vesicle. A cell membrane is simplified as a composite shell of lipid bilayer and membrane skeleton. The membrane skeleton is shown to enhance highly the mechanical stability of cell membranes. In Sec. IV, the application and availability of the elastic theory of low-dimensional continua in nano-structures, including graphene and carbon nanotubes, are discussed. We propose a revised Lenosky lattice model and fit four parameters in this model through the local density approximation. We derive its continuum form up to the second order terms of curvatures and strains, which is the same as the free energy of 2D solid shells. The intrinsic roughening of graphene and several typical mechanical properties of carbon nanotubes are revisited and investigated by using this continuum form. Sec. V is a brief summary and prospect.

II. FUNDAMENTALS OF GEOMETRIC AND ELASTIC THEORY ON LOW-DIMENSIONAL CONTINUA

In this section, we describe the mathematical basis and the elastic theory of 1D and 2D continua.

A. Geometric representation of low-dimensional continua

The 1D continuum (rod) and 2D continuum (membrane or shell) can be expressed as a smooth curve and a smooth surface, respectively.

1. Curve theory

Fig. 1 depicts a curve C embedded in the 3D Euclid space. Each point in the curve can be expressed as a vector \mathbf{r} and let s be the arc length parameter. At point $\mathbf{r}(s)$, one can take \mathbf{T} , \mathbf{N} , and \mathbf{B} as the tangent, normal and binormal vectors, respectively. $\{\mathbf{r}; \mathbf{T}, \mathbf{N}, \mathbf{B}\}$ is called

the Frenet frame which satisfies the Frenet formula:⁴⁷

$$\begin{cases} \mathbf{r}' = \mathbf{T}, \\ \mathbf{T}' = \kappa\mathbf{N}, \\ \mathbf{N}' = (-\kappa\mathbf{T} + \tau\mathbf{B}), \\ \mathbf{B}' = -\tau\mathbf{N}, \end{cases} \quad (1)$$

where the prime represents the derivative with respect to s . κ and τ are the curvature and torsion of the curve, respectively.

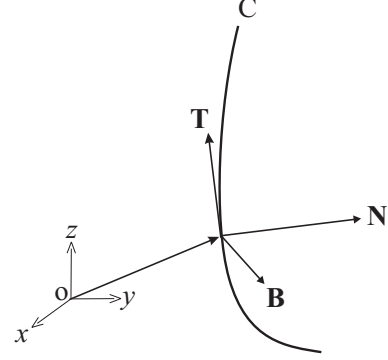


FIG. 1: Frenet frame $\{\mathbf{r}; \mathbf{T}, \mathbf{N}, \mathbf{B}\}$.

The fundamental theory of curve⁴⁷ tells us that the bending and twist properties of a smooth curve are uniquely determined by the Frenet formula (1).

2. Surface theory

Fig. 2 depicts a surface M embedded in the 3D Euclid space. Imagine that a mass point moves on the surface in the speed of unit and that a right-handed frame, which consists of three unit orthonormal vectors with two vectors always in the tangent plane of the surface, adheres to the mass point. Assume that the mass point is at position expressed as vector \mathbf{r} and the frame superposes three unit orthonormal vectors $\{\mathbf{e}_1, \mathbf{e}_2, \mathbf{e}_3\}$ with \mathbf{e}_3 being the normal vector of surface M at some time s . When the mass point moves to another position \mathbf{r}' at time $s + \Delta s$, the frame will superpose three unit orthonormal vectors $\{\mathbf{e}'_1, \mathbf{e}'_2, \mathbf{e}'_3\}$. Thus we call the frame a moving frame and denote it as $\{\mathbf{r}; \mathbf{e}_1, \mathbf{e}_2, \mathbf{e}_3\}$.

If $\Delta s \rightarrow 0$, we define

$$d\mathbf{r} = \lim_{\Delta s \rightarrow 0} (\mathbf{r}' - \mathbf{r}) = \omega_1 \mathbf{e}_1 + \omega_2 \mathbf{e}_2, \quad (2)$$

and

$$d\mathbf{e}_i = \lim_{\Delta s \rightarrow 0} (\mathbf{e}'_i - \mathbf{e}_i) = \omega_{ij} \mathbf{e}_j, \quad (i = 1, 2, 3) \quad (3)$$

where ω_1, ω_2 , and ω_{ij} , ($i, j = 1, 2, 3$) are 1-forms, and ' d ' is the exterior differential operator.^{48,49} Here ω_{12} can be understood as the infinite rotation angle of vectors \mathbf{e}_1 and \mathbf{e}_2 around \mathbf{e}_3 . Similarly, we can understand the physical meaning of the other ω_{ij} . It is easy to obtain $\omega_{ij} = -\omega_{ji}$

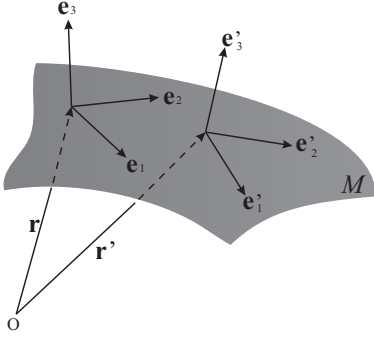


FIG. 2: Moving frame $\{\mathbf{r}; \mathbf{e}_1, \mathbf{e}_2, \mathbf{e}_3\}$ of a surface M .

from $\mathbf{e}_i \cdot \mathbf{e}_j = \delta_{ij}$. Additionally, the structure equations of the surface can be expressed as:^{48,49}

$$\begin{cases} d\omega_1 = \omega_{12} \wedge \omega_2, \\ d\omega_2 = \omega_{21} \wedge \omega_1, \\ d\omega_{ij} = \omega_{ik} \wedge \omega_{kj} \quad (i, j = 1, 2, 3), \end{cases} \quad (4)$$

and

$$\begin{pmatrix} \omega_{13} \\ \omega_{23} \end{pmatrix} = \begin{pmatrix} a & b \\ b & c \end{pmatrix} \begin{pmatrix} \omega_1 \\ \omega_2 \end{pmatrix}, \quad (5)$$

where ‘ \wedge ’ represents the wedge production between two differential forms. The matrix $\begin{pmatrix} a & b \\ b & c \end{pmatrix}$ is the representation matrix of the curvature tensor \mathfrak{R} . Its trace and determinant are two invariants under the coordinate rotation around \mathbf{e}_3 which are denoted by

$$2H = a + c \quad \text{and} \quad K = ac - b^2. \quad (6)$$

They can be expressed as $2H = -(1/R_1 + 1/R_2)$ and $K = 1/R_1 R_2$ by the two principal curvature radii R_1 and R_2 at each point.

Consider a tangent vector \mathbf{m} stemming from \mathbf{r} . Let ϕ be the angle between \mathbf{m} and \mathbf{e}_1 . Then the geodesic curvature, the geodesic torsion, and the normal curvature along the direction of \mathbf{m} can be expressed:⁴⁹

$$\begin{cases} k_g = (d\phi + \omega_{12})/ds, \\ \tau_g = b \cos 2\phi + (c - a) \cos \phi \sin \phi, \\ k_n = a \cos^2 \phi + 2b \cos \phi \sin \phi + c \sin^2 \phi, \end{cases} \quad (7)$$

where ds is the arc length element along \mathbf{m} . If \mathbf{m} aligns with \mathbf{e}_1 , then $\phi = 0$, $k_g = \omega_{12}/ds$, $\tau_g = b$, and $k_n = a$.

B. Elastic theory of 1D continua

We will elucidate the elastic theory of rod with inextensible centerline. As shown in Fig. 3, let us simplify a rod as a curve $\mathbf{r}(s)$ with s being the arc-length parameter, and cut an infinitesimal element (shown in the magnified box) from the rod. There are forces and moments at the

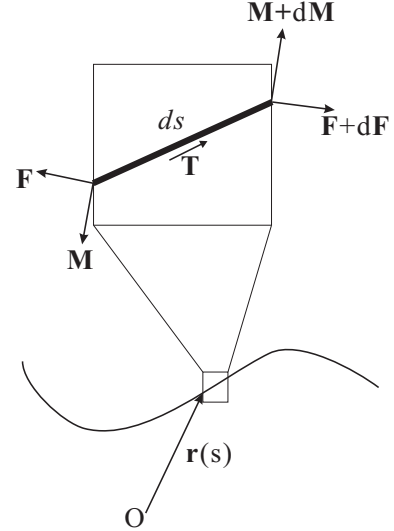


FIG. 3: Force and moment in 1D rod.

two ends of the element which originating from the interaction of other parts of the rod. \mathbf{F} and \mathbf{M} represent the force and moment vectors at point $\mathbf{r}(s)$, while $\mathbf{F} + d\mathbf{F}$ and $\mathbf{M} + d\mathbf{M}$ are the force and moment vectors at point $\mathbf{r}(s + ds)$. From Newton’s laws, we can derive the force and moment balance equations:

$$\sum \mathbf{F} = 0 \Rightarrow \mathbf{F}' = 0, \quad (8)$$

and

$$\sum \mathbf{M} = 0 \Rightarrow \mathbf{M}' + \mathbf{T} \times \mathbf{F} = 0, \quad (9)$$

where the prime represents the derivative with respect to s . One should add the constitutive relation and boundary conditions to make the above two equations closed.

1. Kirchhoff rod theory

A rod with rectangle cross section and centerline C is shown in Fig. 4. Take local coordinates $\{x_1, x_2, x_3\}$ with x_1 and x_2 paralleling respectively to the two edges of the rectangle, and x_3 along the tangent of the centerline. \mathbf{N} is the normal of curve C . Let $\{\mathbf{x}_1, \mathbf{x}_2, \mathbf{x}_3\}$ denote the basis of the local coordinates and define $\kappa_1 = -\mathbf{x}_2 \cdot (d\mathbf{x}_3/ds)$, $\kappa_2 = \mathbf{x}_1 \cdot (d\mathbf{x}_3/ds)$, and $\kappa_3 = \mathbf{x}_2 \cdot (d\mathbf{x}_1/ds)$. Viewed from geometrical point, κ_1 and κ_2 describe the bending of the rod around axes x_1 and x_3 , respectively, and κ_3 represents the twist of the rod around axis x_3 . The free energy density G due to the bending and twist can be expressed as a function of κ_1 , κ_2 , and κ_3 . Expanding G up to the second order terms of κ_1 , κ_2 , and κ_3 , we have

$$G = \gamma + \frac{k_1}{2}(\kappa_1 - \bar{\kappa}_1)^2 + \frac{k_2}{2}(\kappa_2 - \bar{\kappa}_2)^2 + \frac{k_3}{2}(\kappa_3 - \bar{\kappa}_3)^2, \quad (10)$$

where the constant γ can be interpreted as the line tension. $\bar{\kappa}_1$ and $\bar{\kappa}_2$ are interpreted as the spontaneous

curvatures while $\bar{\kappa}_3$ the spontaneous torsion. Denote $\mathbf{k} = \kappa_1 \mathbf{x}_1 + \kappa_2 \mathbf{x}_2 + \kappa_3 \mathbf{x}_3$ and let ϕ be the angle between \mathbf{x}_1 and \mathbf{N} . Then we have

$$\begin{cases} \mathbf{N} = \cos \phi \mathbf{x}_1 - \sin \phi \mathbf{x}_2, \\ \mathbf{B} = \sin \phi \mathbf{x}_1 + \cos \phi \mathbf{x}_2, \end{cases} \quad (11)$$

where \mathbf{B} is the binormal of curve C . From Eqs. (1) and (11), we can derive^{50,51}

$$\mathbf{k} = \kappa \sin \phi \mathbf{x}_1 + \kappa \cos \phi \mathbf{x}_2 + (\tau + \phi') \mathbf{x}_3. \quad (12)$$

Thus G can be also regarded as the function of $\kappa, \tau, \phi, \phi'$.

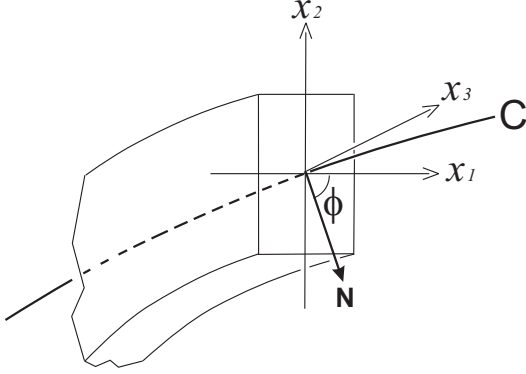


FIG. 4: Rod with rectangle cross section.

The moment vector is defined as²

$$\mathbf{M} = \frac{\partial G}{\partial \mathbf{k}} \equiv \frac{\partial G}{\partial \kappa_1} \mathbf{x}_1 + \frac{\partial G}{\partial \kappa_2} \mathbf{x}_2 + \frac{\partial G}{\partial \kappa_3} \mathbf{x}_3, \quad (13)$$

which is called the constitutive relation. Eqs. (8), (9) and (13) with some boundary conditions form a group of closed equations. They are also available for the rod with cross section different from rectangle if only we take x_1 and x_2 as the two principal axes of inertia. It should be noted that the equivalent form of these equations can be also obtained from the variational method. This method is called the top-down method while the former one via Newton's laws called the bottom-up method.

The free energy of a rod with length L can be written as

$$\mathcal{F} = \int_0^L G(\kappa, \tau; \phi, \phi') ds + \mathcal{F}_{bd}, \quad (14)$$

where \mathcal{F}_{bd} comes from the contributions of two ends of the rod. The general Euler-Lagrange equations corresponding to Eq. (14) are derived as

$$G_\phi - (G_{\phi'})' = 0, \quad (15)$$

$$G_\kappa'' + 2\tau(G_\tau'/\kappa)' + G_\tau' \tau'/\kappa + (\kappa^2 - \tau^2)G_\kappa + 2\kappa\tau G_\tau + \kappa\phi' G_{\phi'} - \kappa G = 0, \quad (16)$$

$$\tau' G_\kappa + 2\tau G_\kappa' - (\kappa G_\tau)' + (\tau^2/\kappa)G_\tau' - (G_\tau'/\kappa)'' = 0, \quad (17)$$

where $G_\phi, G_{\phi'}, G_\kappa$ and G_τ are the partial derivatives of G with respect to ϕ, ϕ', κ and τ , respectively. Additionally, $G_\kappa' \equiv (G_\kappa)'$, $G_\tau' \equiv (G_\tau)'$, $G_\kappa'' \equiv (G_\kappa)''$. The brief

derivation of Eqs. (15)–(17) is attached in Appendix A. These equations have been employed to investigate helical and twisted filaments.¹² There might be a misprint in Eq. (7) of Ref. 12, corresponding to our above equation (17), because the dimension of its last term is different from that of other terms.

Now we would give a typical example to reveal the equivalence relation between Eqs. (8),(9), (13) and Eqs. (15)–(17) rather than prove it directly. Let us consider a rod with $k_1 = k_2 = k_0, k_3 = 0$, and $\bar{\kappa}_1 = \bar{\kappa}_2 = \bar{\kappa}_3 = 0$. The free energy density (10) is simplified as

$$G = (k_0/2)(\kappa_1^2 + \kappa_2^2) + \gamma = (k_0/2)\kappa^2 + \gamma. \quad (18)$$

On the one hand, we have $M_1 = k_0\kappa_1 = k_0\kappa \sin \phi, M_2 = k_0\kappa_2 = k_0\kappa \cos \phi, M_3 = 0$ from Eq. (13). The moment balance equation (9) implies $F_1 = -k_0\kappa_1\kappa_3 - k_0\kappa_2'$ and $F_2 = k_0\kappa_1' - k_0\kappa_2\kappa_3$. Substituting them into the force balance equation (8), we have $F_3 = F_{30} - k_0\kappa^2/2$ and

$$\kappa'' - \kappa\tau^2 + \kappa^3/2 - \kappa F_{30}/k_0 = 0, \quad (19)$$

$$2\tau\kappa' + \kappa\tau' = 0, \quad (20)$$

where F_{30} is an integral constant which represents the line tension of the straight ($\kappa = 0$) rod. On the other hand, we have $G_\kappa = k_0\kappa, G_\phi = G_{\phi'} = G_\tau = 0$. Eq. (15) is trivial while Eqs. (16) and (17) are, respectively, transformed into

$$\kappa'' - \kappa\tau^2 + \kappa^3/2 - \gamma\kappa/k_0 = 0, \quad (21)$$

$$2\tau\kappa' + \kappa\tau' = 0. \quad (22)$$

The above equations are the same as Eqs. (19) and (20) obtained from the force and moment balance conditions if only we take $F_{30} = \gamma$. Thus the equations obtained from the top-down and bottom-up methods are equivalent to each other.

Substituting the free energy density (10) into Eqs. (15)–(17), we obtain the so called shape equations of Kirchhoff rod as

$$(k_1 - k_2)\kappa^2 \sin 2\phi - 2k_3(\tau + \phi')' + 2I_{21}\kappa = 0, \quad (23)$$

$$\begin{aligned} & I_1(2\kappa'' + \kappa^3 - 2\kappa\tau^2) - 2\gamma\kappa + 2I_{12}(\phi'^2 + \tau^2) \\ & + 2I_{21}\phi'' + 2(k_1 - k_2)[(\phi'\kappa \sin 2\phi)'] + \phi'\kappa' \sin 2\phi \\ & - \bar{I}\kappa + 4k_3\tau[(\tau' + \phi'')/\kappa]' + 2k_3(\tau' + \phi'')\tau'/\kappa \\ & + k_3\kappa(\tau + \phi' - \bar{\kappa}_3)(3\tau + \phi' + \bar{\kappa}_3) = 0, \end{aligned} \quad (24)$$

$$\begin{aligned} & I_1(\tau'\kappa + 2\tau\kappa') - k_3[\kappa(\tau + \phi' - \bar{\kappa}_3)]' \\ & + k_3\tau^2(\tau' + \phi'')/\kappa - k_3[(\tau' + \phi'')/\kappa]'' \\ & + 2\tau[(k_1 - k_2)\kappa \sin 2\phi + I_{21}]\phi' - I_{12}\tau' = 0, \end{aligned} \quad (25)$$

where $I_1 = k_1 \sin^2 \phi + k_2 \cos^2 \phi, \bar{I} = k_1 \bar{\kappa}_1^2 + k_2 \bar{\kappa}_2^2, I_{12} = k_1 \bar{\kappa}_1 \sin \phi + k_2 \bar{\kappa}_2 \cos \phi$, and $I_{21} = k_2 \bar{\kappa}_2 \sin \phi - k_1 \bar{\kappa}_1 \cos \phi$.

We also suggest that gentle readers consult the work by Zhou *et al.*¹⁸ where the above equations (23)–(25) and different kinds of boundary conditions are expressed in another representation with the aid of Euler angles.

2. Helfrich rod theory

Helfrich rod theory can be regarded as the fourth order Kirchhoff rod theory with circular cross section to some extent. The free energy density is expressed as⁵²

$$G = \frac{1}{2}k_2\kappa^2 + k_3\kappa^2\tau + \frac{1}{4}k_{22}\kappa^4 + \frac{1}{2}k_4(\kappa'^2 + \kappa^2\tau^2) + \gamma, \quad (26)$$

where k_2 , k_3 , k_{22} and k_4 are elastic constants while γ is the line tension. It is noted that this free energy density is the simplest stable form including the chirality term but without spontaneous curvature and torsion. It has been employed to investigate the circular DNA in Ref. 6 and the Euler-Lagrange equations corresponding to $\int G ds$ are given as:

$$\begin{aligned} & k_2(\kappa^3/2 - \kappa\tau^2 + \kappa'') - \gamma\kappa \\ & + k_3(3\kappa^3\tau - 2\kappa\tau^3 + 6\kappa'\tau' + 2\kappa\tau'' + 6\kappa''\tau) \\ & + k_4(5\kappa^3\tau^2/2 - \kappa\tau^4 + \kappa\kappa'^2/2 - \kappa^2\kappa'' - \kappa'''' \\ & + 6\kappa''\tau^2 + 12\kappa'\tau\tau' + 4\kappa\tau\tau'' + 3\kappa\tau'^2) \\ & + k_{22}(3\kappa^5/4 - \kappa^3\tau^2 + 6\kappa\kappa'^2 + 3\kappa^2\kappa'') = 0, \quad (27) \end{aligned}$$

$$\begin{aligned} & k_2(2\kappa'\tau + \kappa\tau') + k_{22}(\kappa^3\tau' + 6\kappa^2\kappa'\tau) \\ & + k_3(6\kappa'\tau^2 + 6\kappa\tau\tau' - 3\kappa^2\kappa' - 2\kappa''') \\ & + k_4(4\kappa'\tau^3 + 6\kappa\tau^2\tau' - 3\kappa^2\kappa'\tau - \kappa^3\tau' \\ & - 4\kappa'\tau'' - 6\kappa''\tau' - 4\kappa'''\tau - \kappa\tau''') = 0. \quad (28) \end{aligned}$$

Here we will not go on the more higher order Helfrich rod theory, on which gentle readers can consult Refs. 20 and 21.

3. Theory of bending-soften Rod

There are two kinds of rod theory with bending-induced softening. First, let us assume that the bending moment depends linearly on the curvature for small curvature but not on the curvature for large curvature, which is expressed as

$$M = \begin{cases} k_1\kappa, & (\kappa < \kappa_c) \\ k_1\kappa_c, & (\kappa > \kappa_c) \end{cases} \quad (29)$$

where k_1 and κ_c are the elastic bending rigidity and the critical curvature, respectively. Eq. (29) describes the bending-induced softening relation of the first kind which is depicted in Fig. 5(a). The corresponding free energy density can be expressed as

$$G = \gamma + (k_1/2)[\kappa^2 - (\kappa - \kappa_c)^2\mathcal{H}(\kappa - \kappa_c)], \quad (30)$$

where $\mathcal{H}(\cdot)$ is the Heaviside step function. The above form has been employed by Yan *et al.* to investigate the loop formation mechanism and probability of short DNA rings.⁵³ We conjecture that this model could solve the paradox in the experiment on the ring

closure of single-walled carbon nanotubes with 1,3-dicyclohexylcarbodiimide.⁵⁴ Fitting the experiment data with the worm-like chain model,⁵⁵ the persistence length is 800 nm for single-walled carbon nanotubes in the diameter of 1 nm,⁵⁴ which is much smaller than the theoretical value $33 \mu\text{m}$ estimated in terms of the Young's modulus and thickness of single-walled carbon nanotubes in Ref. 44.

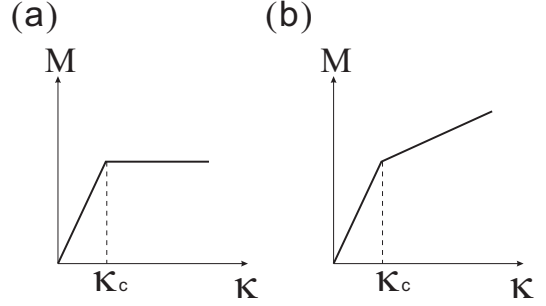


FIG. 5: Bending-induced softening relation: (a) the first kind in expression of Eq. (29); (b) the second kind in expression of Eq. (38).

Consider a rod divided into two parts at $s = L_c$: one part ($s < L_c$) has curvatures less than κ_c another one larger than κ_c . In terms of the variational method in Appendix A, we can derive the equations describing the rod as

$$k_1(2\kappa'' - 2\kappa\tau^2 + \kappa^3) - 2\gamma\kappa = 0 \quad (s < L_c), \quad (31)$$

$$\kappa\tau' + 2\kappa'\tau = 0 \quad (s < L_c), \quad (32)$$

$$k_1\kappa_c(\kappa_c\kappa - 2\tau^2) - 2\gamma\kappa = 0 \quad (s > L_c), \quad (33)$$

$$\tau' = 0 \quad (s > L_c). \quad (34)$$

At the divided point $s = L_c$, we have the joint conditions as

$$\kappa_- = \kappa_+ = \kappa_c, \quad (35)$$

$$\kappa'_- = 0, \quad (36)$$

$$\tau_- = \tau_+, \quad (37)$$

where $(\cdot)_-$ and $(\cdot)_+$ represent the values of (\cdot) at the left and right sides of $s = L_c$.

Secondly, let us assume that the bending moment depends linearly on the curvature for small curvature but weaker linearly on the curvature for large curvature, which is expressed as

$$M = \begin{cases} k_1\kappa, & (\kappa < \kappa_c) \\ k_2(\kappa - \kappa_c) + k_1\kappa_c, & (\kappa > \kappa_c) \end{cases} \quad (38)$$

where $k_1 > k_2$ are the elastic bending rigidities while κ_c is the critical curvature. Eq. (38) describes the bending-induced softening relation of the second kind which is depicted in Fig. 5(b). The corresponding free energy density can be expressed as

$$G = \gamma + (k_1/2)\kappa^2 + [(k_2 - k_1)/2](\kappa - \kappa_c)^2\mathcal{H}(\kappa - \kappa_c), \quad (39)$$

Consider a rod divided into two parts at $s = L_c$: one part ($s < L_c$) has curvatures less than κ_c another one larger than κ_c . In terms of the variational method in Appendix A, we can derive the equations describing the rod as

$$k_1(2\kappa'' - 2\kappa\tau^2 + \kappa^3) - 2\gamma\kappa = 0 \quad (s < L_c), \quad (40)$$

$$\kappa\tau' + 2\kappa'\tau = 0 \quad (s < L_c), \quad (41)$$

$$2k_2\kappa'' + [k_2(\kappa - \kappa_c) + k_1\kappa_c](\kappa^2 - 2\tau^2) - 2\gamma\kappa + (k_2 - k_1)(\kappa - \kappa_c)\kappa\kappa_c = 0 \quad (s > L_c), \quad (42)$$

$$k_2(\tau'\kappa + 2\kappa'\tau) + (k_1 - k_2)\kappa_c\tau' = 0 \quad (s > L_c). \quad (43)$$

At the divided point $s = L_c$, we have the joint conditions as

$$k_1(\kappa_- - \kappa_c) = k_2(\kappa_+ - \kappa_c) \quad (44)$$

$$k_1\kappa'_- = k_2\kappa'_+ \quad (45)$$

$$\tau_- = \tau_+ \quad (46)$$

$$k_1(\kappa_-^2 - \kappa_+^2) = (k_2 - k_1)(\kappa_+ - \kappa_c)^2. \quad (47)$$

Obviously, the above equations (40)–(47) degenerate into Eqs. (31)–(37) if $k_2 = 0$ and into Eqs. (21)–(22) if $k_2 = k_1$.

C. Elastic theory of 2D continua

A 2D continuum can be simplified as a surface as shown in Fig. 6. At each point, we can select a frame $\{\mathbf{e}_1, \mathbf{e}_2, \mathbf{e}_3\}$. A pressure p is loaded on the surface in the inverse direction of the normal vector \mathbf{e}_3 . Let us cut a region enclosed in any curve C from the surface. \mathbf{t} is the tangent vector at point of curve C . \mathbf{b} is normal to \mathbf{t} and in the tangent plane. The force and moment per length performed by the other region on curve C are denoted as \mathbf{f} and \mathbf{m} , respectively. Through Newton's laws, the force and moment balance conditions are obtained as

$$\oint_C \mathbf{f} ds - \int p\mathbf{e}_3 dA = 0, \quad (48)$$

$$\oint_C \mathbf{m} ds + \oint_C \mathbf{r} \times \mathbf{f} ds - \int \mathbf{r} \times p\mathbf{e}_3 dA = 0, \quad (49)$$

where ds and dA are the arc length element of curve C and area element of the region enclosed in curve C , respectively.

Define two second order tensors \mathfrak{S} and \mathfrak{M} such that

$$\mathfrak{S} \cdot \mathbf{b} = \mathbf{f}, \quad \mathfrak{M} \cdot \mathbf{b} = \mathbf{m}. \quad (50)$$

These two tensors can be called as stress tensor and bending moment tensor, respectively. Using the Stokes' theorem, we can derive

$$\int (\text{div } \mathfrak{S} - p\mathbf{e}_3) dA = 0, \quad (51)$$

$$\int (\text{div } \mathfrak{M} + \mathbf{e}_1 \times \mathfrak{S}_1 + \mathbf{e}_2 \times \mathfrak{S}_2) dA = 0. \quad (52)$$

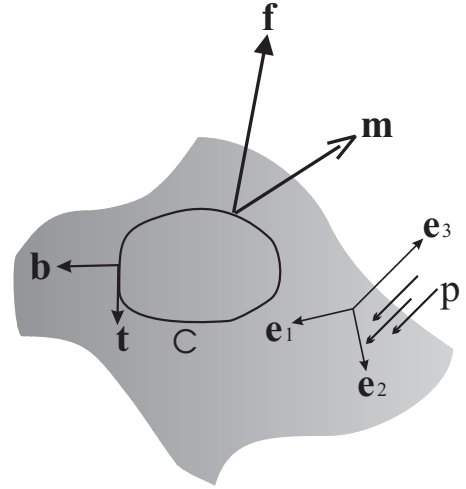


FIG. 6: Force and moment in a 2D continuum.

where $\mathfrak{S}_1 = \mathfrak{S} \cdot \mathbf{e}_1$ and $\mathfrak{S}_2 = \mathfrak{S} \cdot \mathbf{e}_2$. Since the integral is performed on the region enclosed in an arbitrary curve C , from the above two equations we obtain the force and moment balance conditions of 2D continua as:

$$\text{div } \mathfrak{S} = p\mathbf{e}_3, \quad (53)$$

$$\text{div } \mathfrak{M} = \mathfrak{S}_1 \times \mathbf{e}_1 + \mathfrak{S}_2 \times \mathbf{e}_2. \quad (54)$$

The above two equations are equivalent to Eq. (25) in Ref. 56, and Eqs. (28) and (57) in Ref. 57. Eqs. (53) and (54) with some complement constitutive relations form the fundamental equations of 2D continua.

1. Fluid membranes

A fluid membrane is a 2D isotropic continuum which cannot withstand in-plane shear strain. Generally, we assume that the fluid is incompressible. The free energy density, G , of fluid membranes should be invariant under the in-plane coordinate transformation. In terms of the surface theory, there are only two fundamental geometric invariants: the mean curvature $2H$ and gaussian curvature K . Thus the free energy density should be a function of $2H$ and K , that is,

$$G = G(2H, K). \quad (55)$$

The free energy of a closed fluid membrane can be expressed as

$$\mathcal{F} = \int G dA + p \int dV, \quad (56)$$

where dA is the area element of the membrane and dV is the volume element enclosed in the membrane. p is the osmotic pressure, the pressure difference between the outer and inner side of the membrane. The general Euler-Lagrange equation of free energy (56) can be derived

through the variational method shown in Appendix B as

$$p - 2HG + (\nabla^2/2 + 2H^2 - K)(\partial G/\partial H) + (\nabla \cdot \tilde{\nabla} + 2KH)(\partial G/\partial K) = 0. \quad (57)$$

As we known, the above equation has been derived by several authors such as Ou-Yang *et al.*^{49,58} and Giaquinta *et al.*⁵⁹ coming from different research fields. It is recently employed to investigate the modified Korteweg-de Vries surfaces.⁶⁰ Here $\nabla \cdot \tilde{\nabla}$ can be called as the Laplace operator of the second class which is also fully discussed by Zhang and Xu.⁶¹

We emphasize that (57) can be also derived from the bottom-up method, Eqs. (53) and (54) combining a complement constitutive relation

$$\mathfrak{M} = (G_b/2)(\mathbf{e}_1\mathbf{e}_1 - \mathbf{e}_2\mathbf{e}_2) - G_a\mathbf{e}_2\mathbf{e}_1 + G_c\mathbf{e}_1\mathbf{e}_2, \quad (58)$$

where G_a , G_b , and G_c represent the partial derivatives of G with respect to a , b , and c , respectively. Here a , b , and c are the components of the curvature tensor \mathfrak{R} in Eq. (5). To illuminate this point, we consider an example in which the free energy density is taken as $G = k_c(2H)^2 + \lambda$, where k_c and λ are the bending modulus and surface tension of the fluid membrane. It follows that $\mathfrak{M} = 2k_cH(\mathbf{e}_1\mathbf{e}_2 - \mathbf{e}_2\mathbf{e}_1)$ from Eq. (58). Substituting it into Eqs. (53) and (54), we can derive

$$p - 2\lambda H + 4k_cH(H^2 - K) + 2k_c\nabla^2H = 0, \quad (59)$$

which is the same as the result obtained directly from (57). Simultaneously, we have the stress components

$$\mathfrak{S}_1 = (2H^2 - 2aH + \lambda)\mathbf{e}_1 - 2bH\mathbf{e}_2 - 2H_1\mathbf{e}_3, \quad (60)$$

$$\mathfrak{S}_2 = -2bH\mathbf{e}_1 + (2H^2 - 2cH + \lambda)\mathbf{e}_2 - 2H_2\mathbf{e}_3, \quad (61)$$

where H_1 and H_2 are the directional derivatives of H respect to \mathbf{e}_1 and \mathbf{e}_2 . These equations have been also derived by Capovilla and Guven,⁵⁷ from which we seem to arrive at a paradox for fluid membranes: we have mentioned that fluid membranes cannot withstand in-plane shear strain, however Eqs. (60) and (61) reveals shear stress still exhibits in non-spherical vesicles.

2. Solid shells

A solid shell is a 2D isotropic continuum which can endure both bending and in-plane shear strain. The free energy density, G , of solid shells should be invariant under the in-plane coordinate transformation. There are only two fundamental geometric invariants, $2H$ and K , and two fundamental strain invariants: the trace, $2J$, and the determinate, Q , of the in-plane strain tensor. Thus free energy density should be a function of $2H$, K , $2J$, and Q . That is, $G = G(2H, K; 2J, Q)$.

If the solid shell has no initial strains and consists of materials distributing symmetrically with regard to the

middle surface of the shell, we can expand G up to the second order terms of curvatures and strains as

$$G = (k_c/2)(2H)^2 - \bar{k}K + (k_d/2)(2J)^2 - \tilde{k}Q, \quad (62)$$

where k_c and \bar{k} are the bending moduli while k_d and \tilde{k} are the in-plane rigidity moduli. The theory based on the above free energy density is called Kirchhoff's linear shell theory.² Especially, if the shell consists of 3D isotropic materials, we have

$$k_c = Yh^3/12(1 - \nu^2), \quad (63)$$

$$k_d = Yh/(1 - \nu^2), \quad (64)$$

$$\bar{k}/k_c = \tilde{k}/k_d = (1 - \nu), \quad (65)$$

where Y and ν are the Young's modulus and Poisson ratio while h is the thickness of the shell.³

For a closed shell, its free energy is expressed as Eq. (56) with G in Eq. (62). Of course, we can obtain the equations of in-plane strains and shapes through the variational method in Appendix B. The final results are the same as those obtained from Eqs. (53) and (54) with a complement constitutive relations (58) and

$$\mathfrak{S} = \mathfrak{S}^i + \mathfrak{S}^f \quad (66)$$

with

$$\mathfrak{S}^i \equiv G_{\varepsilon_{11}}\mathbf{e}_1\mathbf{e}_1 + (G_{\varepsilon_{12}}/2)(\mathbf{e}_1\mathbf{e}_2 + \mathbf{e}_2\mathbf{e}_1) + G_{\varepsilon_{22}}\mathbf{e}_2\mathbf{e}_2, \quad (67)$$

where $G_{\varepsilon_{11}}$, $G_{\varepsilon_{12}}$, and $G_{\varepsilon_{22}}$ represent the partial derivatives of G with respect to ε_{11} , ε_{12} , and ε_{22} , the components of the in-plane strain tensor \mathfrak{E} . Substituting Eq. (62) into Eqs. (58) and (67), and then employing Eqs. (53) and (54), we obtain

$$d(\mathfrak{S}_{11}^i\omega_2 - \mathfrak{S}_{12}^i\omega_1) - (\mathfrak{S}_{21}^i\omega_2 - \mathfrak{S}_{22}^i\omega_1) \wedge \omega_{21} = 0, \quad (68)$$

$$d(\mathfrak{S}_{21}^i\omega_2 - \mathfrak{S}_{22}^i\omega_1) - (\mathfrak{S}_{11}^i\omega_2 - \mathfrak{S}_{12}^i\omega_1) \wedge \omega_{12} = 0, \quad (69)$$

and

$$p + 2k_c[2H(H^2 - K) + \nabla^2H] - 4(k_d - \tilde{k})JH - \tilde{k}\mathfrak{R} : \mathfrak{E} = 0, \quad (70)$$

where $\mathfrak{S}_{11}^i = (2k_dJ - \tilde{k}\varepsilon_{22})$, $\mathfrak{S}_{12}^i = \mathfrak{S}_{21}^i = \tilde{k}\varepsilon_{12}$, and $\mathfrak{S}_{22}^i = (2k_dJ - \tilde{k}\varepsilon_{11})$ are the components of tensor \mathfrak{S}^i . \mathfrak{R} is the curvature tensor related to Eq. (5). The above equations (68)–(70) describe the in-plane strains and shapes of solid shells at equilibrium state. The similar equations and the corresponding dynamics forms have been derived through the variational method in Refs. 49 and 62, respectively, with the aid of moving frame method.

The above equations (68) and (69) can be written as one vector equation by introducing a displacement vector $\mathbf{u} = u_1\mathbf{e}_1 + u_2\mathbf{e}_2 + u_3\mathbf{e}_3$, which is related to two invariants $2J$ and Q of the in-plane strain tensor as

$$2J = \text{div } \mathbf{u} - 2Hu_3 \quad (71)$$

$$2Q = (\text{div } \mathbf{u} - 2Hu_3)^2 + (1/2)(\text{curl } \mathbf{u})^2 - (\diamond \mathbf{u})^2, \quad (72)$$

where $\diamond\mathbf{u} = \nabla\mathbf{u} - \mathbf{e}_3(\mathbf{e}_3 \cdot \nabla\mathbf{u})$ is the in-plane part of $\nabla\mathbf{u}$. Using the new variable \mathbf{u} , Eqs. (68) and (69) can be written as

$$(\tilde{k} - 2k_d)\nabla(\text{div}\mathbf{u} - 2Hu_3) - \tilde{k}(\diamond^2\mathbf{u} + K\bar{\mathbf{u}} + \tilde{\nabla}u_3) = 0, \quad (73)$$

where $\bar{\mathbf{u}}$ and $\diamond^2\mathbf{u}$ are the in-plane components of \mathbf{u} and $\text{div}(\diamond\mathbf{u})$, respectively. $\tilde{\nabla}$ is called the gradient operator of the second class, which is shown in our previous work.⁴⁹ In particular, H , K , $\tilde{\nabla}u_3$ vanish and \diamond^2 degenerates into ∇^2 for a flat manifold. Then the above equation degenerates into the Cauchy equation² in 2D plane. Thus Eq. (73) can be regarded as the Cauchy equation in a curved surface.

III. APPLICATION OF ELASTIC THEORY IN BIO-STRUCTURES

In the above section, we have described fundamentals of geometric and elastic theory on low-dimensional continua. Can this theory be applied to the bio-structures, such as DNA and cell membranes, and so on? DNA is a long chain macromolecule which may be described as an elastic rod. A cell membrane is a thin structure whose thickness and the size of the microscopic components are so much smaller than its lateral dimension that it can be regarded as a 2D continuum phenomenologically. We will discuss the application of the above elastic theory in short DNA rings, lipid membranes and cell membranes in this section.

A. Short DNA ring

DNA is a double helical structure whose diameter is about 2.5 nm. Its bending rigidity, described as the persistence length l_p , is about 50 nm (150 bp) at the room temperature. The normal DNA is usually flexible enough because its length is so much larger than l_p that the fluctuations are quite evident. Thus the rod theory cannot directly be applied to the normal DNA. The statistical theory combining the rod theory is required,^{63,64} which is out of our topic in this review. However, there is a special kind of short DNA rings^{65,66,67} which are in the length scale of l_p so that the fluctuation effect can be neglected. The diameter is still much smaller than the total length. Thus the rod theory mentioned in Sec. II B is expected to be available for this kind of DNA rings.

Han *et al.* have used AFM to observe DNA rings consisting of several segments connected by kinks in the presence of Zn^{2+} ions.^{65,66} Zhao *et al.* have analyzed the mechanism of this kink instability based on Helfrich rod theory.⁶ Their main ideas are sketched as follows. First, a circle is a solution to Eqs. (27) and (28). Next, through analyzing the stability of the cycle, it is found that, for the given elastic constants, there exists a critical radius above which DNA circles will be instable. This prediction is in good agreement with the experiments,^{65,66} where

kink deformations were observed in DNA rings of 168 bp but not 126 bp. Above some thresholds of the chiral modulus, k_3 in Eq. (26), the DNA circles turn into elliptical, triangular, square, or other polygonal shapes, respectively. This fact agrees with the experiments if k_3 is positively correlated to the condensation of Zn^{2+} ions.

Interestingly, Zhou and Ou-Yang proposed another interpretation based on the dynamic instability of Kirchhoff rod theory⁸ with $\bar{\kappa}_2 = \bar{\kappa}_3 = 0$ in Eq. (10). Their result is the same as that obtained directly from the first and second order variations of the free energy. We deal with the latter scenario. First, $\tau = 0$, $\phi = 0$, and $\kappa = 1/R$ satisfy Eqs. (23)–(25) derived from the first order variation of the free energy. That is, a planar circle with radius R is an equilibrium configuration. Next, through the second order variation of the free energy, we can obtain the characteristic function describing the stability of the circle

$$g_c(R) = \bar{\kappa}_1^2 - (1 - \Gamma)\bar{\kappa}_1/R - \Gamma n^2/R^2 \leq 0 \quad (74)$$

where $n > 1$ is an arbitrary integer and $\Gamma = k_3/k_1$. From the above inequality, we obtain the critical radius

$$R_c = 8\Gamma/\bar{\kappa}_1[\Gamma - 1 + \sqrt{(\Gamma - 1)^2 + 16\Gamma}], \quad (75)$$

above which the circle is instable. If only the presence of Zn^{2+} ions tunes the values of Γ and k_3/k_2 such that R_c is in the range between $63/\pi$ (bp) and $84/\pi$ (bp), the above result is also in agreement with the experiments,^{65,66} where kink deformations were observed in DNA rings of 168 bp but not 126 bp.

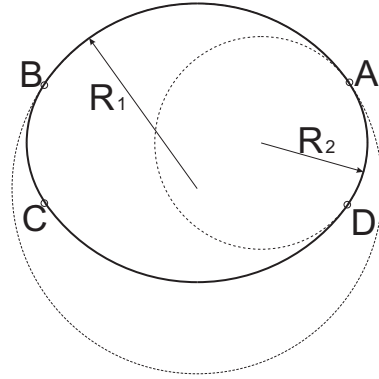


FIG. 7: A possible configuration of a short DNA ring.

In Sec. II B, we also mention the theory of bending-soften rod. Can this theory also provide an interpretation to the experiments? Let us consider the bending-soften rod theory of the first kind whose free energy density is expressed as Eq. (30). When the radius R of the ring is smaller than $1/\kappa_c$, any small perturbation will increase the free energy. If $R > 1/\kappa_c$, the ring might transform into the fictitious configuration shown in Fig. 7 which consists of four arcs AB, BC, CD, DA with the radius R_1 and R_2 . To see conveniently, the joint points are marked as small circles in the figure. Obviously, $R_2 < R < R_1$.

Through simple calculations, we find that the fictitious configuration is energetically less favorable than the perfect ring with radius R . Therefore, this coarse analysis reveals that the theory of bending-soften rod cannot explain the experiments.

B. Lipid membrane

Lipids are dominant composition of cell membranes. Most of lipid molecules have a polar hydrophilic head group and two hydrophobic hydrocarbon tails. When a quantity of lipid molecules disperse in water, they will assemble themselves into a bilayer vesicle as depicted in Fig. 8, in which the hydrophilic heads shield the hydrophobic tails from the water surroundings because of the hydrophobic forces. This self-assembly process has been numerically investigated by Lipowsky *et al.*^{68,69,70} and Noguchi *et al.*⁷¹ through molecular dynamics simulation based on coarse-grained model or meshless membrane model.

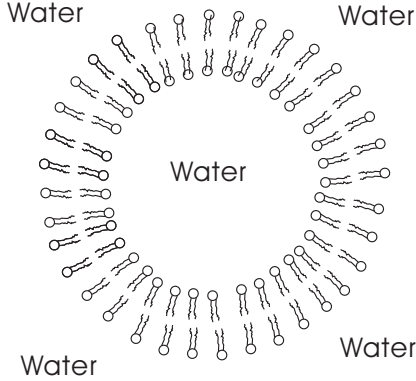


FIG. 8: A lipid bilayer vesicle.

The thickness of the lipid bilayer and the size of single lipid molecules are much smaller than the scale of the whole lipid bilayer. Additionally, at the physiological temperature, the lipid bilayer is usually at the nematic state where the hydrocarbon chains of the lipid molecules are roughly perpendicular to the bilayer surface. Thus the bilayer can be regarded as a 2D fluid membrane whose free energy density is expressed as Eq. (55). Expanding it up to the second order terms of curvatures, we obtain the Helfrich's form:²⁹

$$G_H = (k_c/2)(2H + c_0)^2 - \bar{k}K + \lambda, \quad (76)$$

where k_c and \bar{k} are the bending moduli of the lipid bilayer. We emphasize that the minus sign before \bar{k} in Eq. (76) is opposite to Helfrich's convention. λ is the surface tension of the bilayer. c_0 is called the spontaneous curvature that reflects asymmetric factors between two sides of the bilayer, including the lipid distribution, the chemical environment, and so on. k_c is about 20 T for lipid bilayers, where the Boltzmann factor is set to 1

and T the room temperature, from which the persistence length of lipid bilayers is estimated about $10 \mu\text{m}$.^{32,33} In this section we only consider the size of lipid bilayers smaller than $10 \mu\text{m}$ so that the fluctuation effect on the shape of lipid bilayers can be neglected. The model based on Eq. (76) is called spontaneous curvature model. We still remind gentle readers to note the two similar non-local models—the bilayer-coupling model^{72,73} and the area difference model,⁷⁴ although we will not touch them in the present review.

1. Closed vesicles

The free energy of a lipid vesicle under the osmotic pressure p (the outer pressure minus the inner one) can be written as Eq. (56) with $G = G_H$ being Helfrich's form (76). Substituting (76) into Eq. (57), we can obtain the shape equation of lipid vesicles:^{75,76}

$$p - 2\lambda H + k_c(2H + c_0)(2H^2 - c_0H - 2K) + 2k_c\nabla^2 H = 0. \quad (77)$$

This equation is the fourth order nonlinear equation. It is not easy to find its special solutions. We have known three typical analytical solutions: sphere,⁷⁵ torus,^{77,78} and biconcave discoid shape.⁷⁹

For a sphere with radius R , we have $H = -1/R$ and $K = 1/R^2$. Substituting them into (77), we arrive at

$$pR^2 + 2\lambda R - k_c c_0(2 - c_0 R) = 0. \quad (78)$$

This equation gives the sphere radius under the osmotic pressure p .

A torus is a revolution surface generated by a circle with radius ρ rotating around an axis in the same plane of the circle. The revolution radius r should be larger than ρ . A point in the torus can be expressed as a vector $\{(r + \rho \cos \varphi) \cos \theta, (r + \rho \cos \varphi) \sin \theta, \rho \sin \varphi\}$. Through simple calculations, we have $2H = -(r + 2\rho \cos \varphi)/\rho(r + \rho \cos \varphi)$, $K = \cos \varphi/\rho(r + \rho \cos \varphi)$. Substituting them into Eq. (77), we derive

$$\begin{aligned} & [(2k_c c_0^2 \rho^2 - 4k_c c_0 \rho + 4\lambda \rho^2 + 2P\rho^3)/\varrho^3] \cos^3 \varphi \\ & + [(5k_c c_0^2 \rho^2 - 8k_c c_0 \rho + 10\lambda \rho^2 + 6P\rho^3)/\varrho^2] \cos^2 \varphi \\ & + [(4k_c c_0^2 \rho^2 - 4k_c c_0 \rho + 8\lambda \rho^2 + 6P\rho^3)/\varrho] \cos \varphi \\ & + 2k_c/\varrho^2 + k_c(c_0^2 \rho^2 - 1) + 2(P\rho + \lambda)\rho^2 = 0, \end{aligned} \quad (79)$$

where $\varrho = r/\rho$. If ϱ is finite, then Eq. (79) holds if and only if the coefficients of $\{1, \cos \varphi, \cos^2 \varphi, \cos^3 \varphi\}$ vanish. It follows $2\lambda \rho^2 = k_c c_0 \rho(4 - c_0 \rho)$, $P\rho^3 = -2k_c \rho c_0$ and $\varrho = \sqrt{2}$.⁷⁷ That is, there exists a lipid torus with the ratio of its two generated radii being $\sqrt{2}$, which was confirmed in the experiment 80.

To describe the solution of biconcave discoid shape, we write the shape equation (77) under the axisymmetric condition. If a planar curve $z = z(\rho)$ revolves around the z -axis, an axisymmetric surface is formed. Each point on the surface is expressed as $\mathbf{r} = \{\rho \cos \varphi, \rho \sin \varphi, z(\rho)\}$.

Denote $\psi = \arctan(dz/d\rho)$ and $\Psi = \sin \psi$. Then Eq. (77) is transformed into⁸¹

$$\frac{1}{2} \left[\frac{(\rho\Psi)'}{\rho} + c_0 \right] \left\{ \left[\rho \left(\frac{\Psi}{\rho} \right)' \right]^2 - \frac{c_0(\rho\Psi)'}{\rho} \right\} - \frac{\lambda(\rho\Psi)'}{k_c\rho} + \left\{ \rho \left[\frac{(\rho\Psi)'}{\rho} \right]' \right\} \frac{1 - \Psi^2}{\rho} - \left[\frac{(\rho\Psi)'}{\rho} \right]' \Psi\Psi' + \frac{p}{k_c} = 0, \quad (80)$$

where the prime represents the derivative with respect to ρ . This equation is called the shape equation of axisymmetric lipid vesicles. Its first integral, group structure and corresponding Hamilton's equations are investigated by Zheng and Liu,⁸² Xu and Ou-Yang,⁸³ and Capovilla et al.^{84,85} respectively.

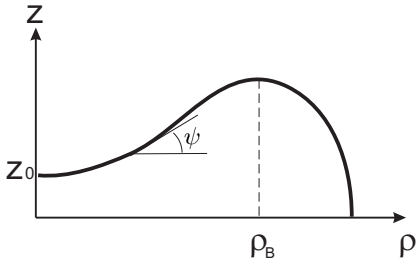


FIG. 9: A quarter outline of the biconcave surface.

It is easy to verify that $\Psi = \sin \psi = -c_0\rho \ln(\rho/\rho_B)$ with a constant ρ_B is a solution to Eq. (80) if p and λ are vanishing. For $0 < c_0\rho_B < e$, the parameter equation

$$\begin{cases} \sin \psi = -c_0\rho \ln(\rho/\rho_B) \\ z = z_0 + \int_0^\rho \tan \psi d\rho \end{cases} \quad (81)$$

corresponds to a curve shown in Fig. 9. A biconcave discoid surface will be achieved when this curve revolves around z -axis and then reflects concerning the horizontal plane. The above equation (81) can give a good explanation to the shape of human red blood cell under normal physiological conditions.⁷⁹ If $c_0\rho_B$ is out of the range between 0 and e , Eq. (81) corresponds to a prolate ellipsoid or other self-intersecting surfaces.⁸⁶

In the purely mathematical viewpoint, there are also the other solutions to Eq. (77) such as cylinder, constant mean curvature surface, periodic undulation surface,⁸⁷ pearling tubule,⁸⁸ and so on.^{34,89} However, It is a pity that they are open surfaces and do not correspond to truly closed vesicles.

As mentioned above, it is fairly difficult to find the analytical solution to Eq. (77). Thus we appreciate the applications of numerical methods to find the equilibrium shapes of closed vesicles. Two kinds of typical numerical frameworks are usually employed. The first one is to use 'Surface Evolver', a software package developed by Brakke,⁹⁰ to find the configurations minimizing the free energy under some constraints.^{91,92,93,94} The second one is based on the phase field formulation of Helfrich's free energy density (76) and diffusive interface approximation.^{95,96,97,98} The above numerical methods

can obtain lipid vesicles with different shapes either axisymmetric or asymmetric. Additionally, the finite element method might be a potential method although very sparse literature⁹⁹ treats lipid bilayers by using it.

2. Stability of closed vesicles

When the osmotic pressure is beyond some threshold, a closed vesicle will lose its stability and change its shape abruptly. The threshold is called the critical pressure. To obtain it, one should calculate the second order variation of the free energy (56) with G being Helfrich's form (76), which has been dealt with in the general case as:^{49,100}

$$\begin{aligned} \delta^2 \mathcal{F} = & \int k_c [(\nabla^2 \Omega_3)^2 + (2H + c_0) \nabla(2H\Omega_3) \cdot \nabla \Omega_3] dA \\ & + \int [4k_c(2H^2 - K)^2 + k_c K(c_0^2 - 4H^2) + 2\lambda K - 2Hp] \Omega_3^2 dA \\ & + \int [k_c(14H^2 + 2c_0H - 4K - c_0^2/2) - \lambda] \Omega_3 \nabla^2 \Omega_3 dA \\ & - 2k_c \int (2H + c_0) [\nabla \Omega_3 \cdot \tilde{\nabla} \Omega_3 + 2\Omega_3 \nabla \cdot \tilde{\nabla} \Omega_3] dA, \end{aligned} \quad (82)$$

where Ω_3 is an arbitrary small out-of-plane displacement and the operator $\tilde{\nabla}$ is the gradient operator of the second class.⁴⁹

Here we will mention two results for special configurations.

First, let us consider a lipid sphere that satisfies Eq. (78). On the sphere, the function Ω_3 can be expanded by the spherical harmonic functions Y_{lm} as $\Omega_3 = \sum_{l=0}^{\infty} \sum_{m=-l}^{m=l} a_{lm} Y_{lm}$. Substituting it into Eq. (82), we derive $\delta^2 \mathcal{F} = (R/2) \sum_{l,m} |a_{lm}|^2 [l(l+1) - 2] \{2k_c[l(l+1) - c_0R]/R^3 - p\}$, From which we can obtain the critical pressure⁷⁵

$$p_c = 2k_c(6 - c_0R)/R^3. \quad (83)$$

If $p < p_c$, $\delta^2 \mathcal{F} \geq 0$ for any $|a_{lm}|$; on the contrary, $\delta^2 \mathcal{F}$ can be negative for the special selection of $|a_{lm}|$. The above equation depends also on c_0 . If $c_0 > 6/R$, then p_c is negative, which reveals that a sphere vesicle is always unstable for large enough c_0 .

Next, let us still regard a long enough lipid tubule as a closed vesicle. Denoted its radius as ρ . From Eq. (77) we have

$$(k_c/2)(1/\rho^2 - c_0^2) - p\rho = \lambda. \quad (84)$$

On the cylindrical surface, Ω_3 can be expanded as Fourier series $\Omega_3 = \sum_{l=-\infty}^{\infty} a_l \exp(il\theta)$. Substituting it into Eq. (82) and combining Eq. (84), we derive $\delta^2 \mathcal{F} = \sum_{l=-\infty}^{\infty} |a_l|^2 (l^2 - 1) [k_c(l^2 - 1)/\rho^3 - p]$, From which we can obtain the critical pressure

$$p_c = 3k_c/\rho^3. \quad (85)$$

If $p < p_c$, $\delta^2 \mathcal{F} \geq 0$ for any $|a_l|$; on the contrary, $\delta^2 \mathcal{F}$ can be negative for the special selection of $|a_l|$.

3. Open vesicles with free edges

The opening-up process of lipid vesicles by talin, a protein, has recently been observed^{101,102} which pushes us to study the equilibrium equation and boundary conditions of lipid vesicles with free exposed edges. Capovilla *et al.* have addressed this problem and given the equilibrium equation and boundary conditions.¹⁰³ Inspired by the talk “moving frame method” of Chern,¹⁰⁴ we introduce exterior differential form to deal with the variational problem on open surface and obtain concisely the shape equation and boundary conditions of open lipid vesicles.¹⁰⁵ Numerical solution to the shape equation and boundary conditions with relaxed method can explain the experimental results very well.¹⁰⁶ A quantity of open vesicles with free edges have also been obtained numerically by Wang and Du¹⁰⁷ with the phase field method. Here we will not further discussed the dynamical opening process of the vesicles, which has been recently investigated by Kaga and Ohta.¹⁰⁸

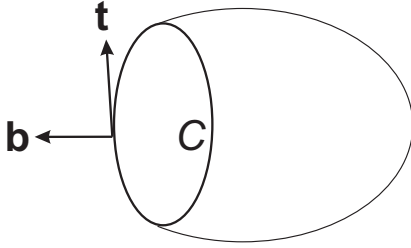


FIG. 10: An open surface with boundary curve C .

We regard an open lipid vesicle with a free edge as a smooth surface with a boundary curve C , as shown in Fig. 10. \mathbf{t} is the tangent vector of the curve C . \mathbf{b} , in the tangent plane of the surface, is perpendicular to \mathbf{t} and points to the opposite side that the surface located in. The free energy of the open lipid vesicle is written as

$$\mathcal{F} = \int G_H dA + \gamma \oint_C ds, \quad (86)$$

where γ represents the line tension of the edge and G_H has the Helfrich's form (76).

The first order variation of \mathcal{F} gives the shape equation

$$k_c(2H+c_0)(2H^2-c_0H-2K)-2\lambda H+2k_c\nabla^2 H=0, \quad (87)$$

and the boundary conditions as:¹⁰⁵

$$[k_c(2H+c_0)-\bar{k}k_n]_C=0, \quad (88)$$

$$[2k_c\partial H/\partial\mathbf{b}+\gamma k_n-\bar{k}\tau'_g]_C=0, \quad (89)$$

$$[G_H+\gamma k_g]_C=0, \quad (90)$$

where k_n and k_g are normal curvature and geodesic curvature of the boundary curve C . τ'_g is the derivative of geodesic torsion τ_g with respect to the arc length of curve C . The mechanical meanings of the above four equations

are as follows: Eq. (87) is the normal force balance equation of the membrane; Eq. (88) is the moment balance equation of points in curve C around the direction of \mathbf{t} ; Eq. (89) is the force balance equation of points in curve C along the normal direction of surface; and Eq. (90) is the force balance equation of points in curve C along the direction of \mathbf{b} . It is necessary to emphasize that the boundary conditions are available for open vesicles with more than one free edge because the edge in our derivation is a general one.

In Ref. 105, we have shown two analytical solutions to above equations (87)–(90): One is a cup-like membrane and another is the central part of a torus. Several numerical solutions to these equations are obtained by Umeda *et al.*¹⁰⁶. Their results reveal that the line tension γ induced by talin correlates negatively with the concentration of talin, which is in agreement with the experimental result that the hole of vesicle is enlarged with the concentration of talin.¹⁰¹

4. Vesicles with lipid domains

The above discussion on open lipid vesicles with free edges can be extended to study a vesicle of several lipid components. The domains usually formed so that each domain contains one or two kinds of lipid molecules. The morphology of axisymmetric vesicles with multidomains has been theoretically investigated by Jülicher and Lipowsky.¹⁰⁹ It is found that lipid domains facilitate the budding of vesicles.¹¹⁰ The giant vesicles with lipid domains have been observed in recent experiment.¹¹¹ There are two kinds of lipid domains which are at the liquid-ordered state and liquid-disordered state, respectively. It is natural to assume that different kinds of domains have different bending moduli and spontaneous curvatures. The axisymmetric vesicles in the experiment can be explained with Jülicher-Lipowsky theory through numerically method. Baumgart *et al.* have demonstrated that the line tension, the osmotic pressure, the relative bending moduli, and the spontaneous curvature have significant effects on the morphology of a vesicle with two domains being at the liquid-ordered and disordered states, respectively.¹¹²

The asymmetric vesicles are also experimentally observed in Ref. 111, which enlightens us to investigate the shape equation of each domains and the boundary conditions between domains without any axisymmetric assumptions. Let us consider a vesicle with two domains separated by curve C sketched in Fig. 11. The free energy can be expressed as¹⁰⁹

$$\mathcal{F} = \int G_H^I dA + \int G_H^{II} dA + \gamma \oint ds + p \int dV, \quad (91)$$

where G_H^I and G_H^{II} have the Helfrich from (76) with the bending moduli k_c^I , \bar{k}^I , k_c^{II} , \bar{k}^{II} , the spontaneous curvatures c_0^I , c_0^{II} , and the surface tensions λ^I , λ^{II} , respectively. The integrals in the first and second terms of

Eq. (91) are performed on the domain I and II shown in Fig. 11, respectively. γ is the line tension of boundary curve C . p is the osmotic pressure of the vesicle.

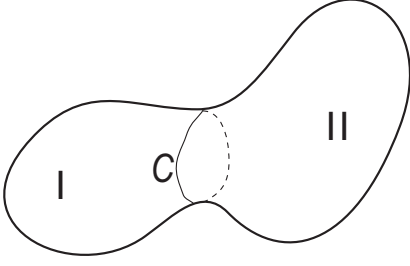


FIG. 11: A vesicle with two domains separated by curve C .

In terms of the physical meanings of Eqs. (87)–(90), we can easily write down the shape equation of domains as:^{49,113}

$$p - 2\lambda^i H + k_c^i (2H + c_0) (2H^2 - c_0^i H - 2K) + 2k_c^i \nabla^2 H = 0. \quad (92)$$

where the superscript $i = I$ and II represents the physical quantity of lipid domains I and II, respectively. Additionally, the boundary conditions between domains are as follows:^{49,113}

$$[k_c^I (2H + c_0^I) - k_c^{II} (2H + c_0^{II}) - (\bar{k}^I - \bar{k}^{II}) k_n]_C = 0, \quad (93)$$

$$[2(k_c^I + k_c^{II}) \partial H / \partial \mathbf{b} - (\bar{k}^I + \bar{k}^{II}) \tau'_g + \gamma k_n]_C = 0, \quad (94)$$

$$[G^I - G^{II} + \gamma k_g]_C = 0, \quad (95)$$

where \mathbf{b} is perpendicular to the boundary curve C and points to the side of domain II.

As we know, there is still no any numerical result on asymmetric vesicles with domains directly from the above equations in the previous literature. Only in Ref. 107, Wang and Du discussed the morphology of asymmetric vesicles with domains through the phase field model.

In the above theory, the detailed architecture of liquid-ordered and disordered phases is neglected. There are special lipid domains at liquid-ordered phase, so called rafts, which are enriched in cholesterol and sphingolipids.¹¹⁴ Cholesterol is a kind of chiral molecules, which has not been included in the above theory. Recently, a concise theory of chiral lipid membranes developed by Tu and Seifert¹¹⁵ might be extended to discuss the raft domains.

5. Adhesions of Vesicles

Cell adhesion is a complex biological process which controls many functions of life. It can be understood as a first-order wetting transition¹¹⁶ and might be simplified as the adhesion of lipid vesicles. As a model, Seifert and Lipowsky have theoretically investigated a lipid vesicle adhering to a flat rigid substrate and found that the vesicle undergoes a nontrivial adhesion transition from the free state to the bound state, which is governed

by the competition between the bending and adhesion energies.¹¹⁷ Ni *et al.* have discussed the adhering lipid vesicles with free edges and the adhesion between a lipid tubule with a rigid substrate.^{118,119} A big progress on this topic is recently made by Guven and his coworkers^{120,121} who obtain the general equations to describe the contact line between the vesicle and the rigid substrate or another vesicle.

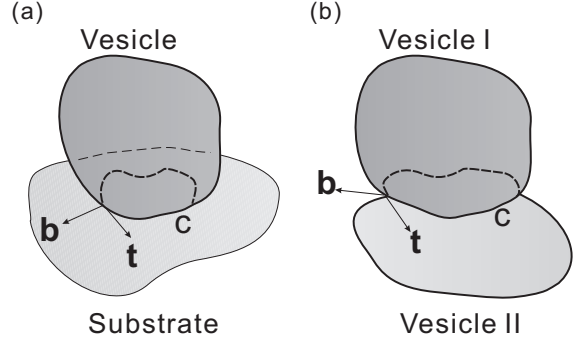


FIG. 12: Adhesions. (a) Adhesion between a lipid vesicle and rigid substrate with a contact line C . (b) Adhesion between two lipid vesicles with a contact line C .

The adhesion between a lipid vesicle and a rigid substrate is depicted in Fig. 12a where the contact area is denoted by \bar{A} . The free energy of this system is expressed as¹¹⁷

$$\mathcal{F} = \int G_H dA + p \int dV - W \bar{A}, \quad (96)$$

where p is the osmotic pressure of the vesicle and W is the strength of the adhesion potential between the vesicle and the substrate. G_H is the free energy density of Helfrich's form (76). For the flat rigid substrate, a characteristic radius and the length scale of the vesicle are defined as $R_a = \sqrt{2k_c/W}$ and $R = \sqrt{A/4\pi}$, respectively. If $R < R_a$, the vesicle is a little stiffer or the attraction is relative weak such that \bar{A} approaches to zero. Thus the vesicle is unbound to the substrate and this state is called the free state. On the contrary, the vesicle is at the bound state. At this state, let us take \mathbf{t} as the tangent vector of the contact line C , and \mathbf{b} perpendicular to \mathbf{t} and in the common tangent plane of the lipid vesicle and the substrate. The absolute value of the normal curvature along \mathbf{b} for the point on the contact line is proven to be $\sqrt{2W/k_c}$ for an axisymmetric vesicle adhering to the flat substrate.¹¹⁷ If the rigid substrate is curved, the above conclusion is revised as¹²¹

$$|\kappa_{\mathbf{b}}^V - \kappa_{\mathbf{b}}^S| = \sqrt{2W/k_c}, \quad (97)$$

where $\kappa_{\mathbf{b}}^V$ and $\kappa_{\mathbf{b}}^S$ are the normal curvatures along \mathbf{b} for the points outside but near the contact line, calculated by using the surfaces of the vesicle and the substrate, respectively.

The adhesion between two lipid vesicles is depicted in Fig. 12b. The free energy of this system is expressed

as¹¹⁷

$$\mathcal{F} = \int G_H^I dA + \int p^I dV + \int G_H^{II} dA + \int p^{II} dV - W\bar{A}, \quad (98)$$

where p^I and p^{II} are the osmotic pressures of the vesicles I and II, respectively. \bar{A} and W are the contact area and adhesion strength, respectively. G_H^I and G_H^{II} are the Helfrich's free energy density of vesicle I and II. The first order variation of (98) gives the same shape equation of two vesicles as (92) and the adhesion boundary conditions:¹²¹

$$(1 + k_c^I/k_c^{II})(\kappa_{\mathbf{b}}^I - \kappa_{\mathbf{b}}^A)^2 = 2W/k_c^I, \quad (99)$$

$$(1 + k_c^{II}/k_c^I)(\kappa_{\mathbf{b}}^{II} - \kappa_{\mathbf{b}}^A)^2 = 2W/k_c^{II}, \quad (100)$$

$$\partial(\kappa_{\mathbf{b}}^I + \kappa_{\mathbf{b}}^{II} - \kappa_{\mathbf{b}}^A)/\partial\mathbf{b} = 0, \quad (101)$$

where $\kappa_{\mathbf{b}}^I$ and $\kappa_{\mathbf{b}}^{II}$ are the normal curvatures along \mathbf{b} for the points outside the adhesion domain but near the contact line calculated by using the surfaces of vesicles I and II, respectively. $\kappa_{\mathbf{b}}^A$ is the normal curvature for the points inside the adhesion domain but near the contact line calculated by using the common surface of vesicles I and II. As we know, there is still lack of numerical solutions to the above equations (99)–(101) in the previous literature. Only in the recent work, Zihel and Svetina¹²² have investigated the adhesion between two vesicles by numerically minimizing the free energy (98) with $k_c^{II} = k_c^I$ and various W .

Is the behavior of vesicle adhesion close to that of cell adhesion? The cell membrane can bear shear strain whose adhesion behavior might be much closer to the adhesion between a polyelectrolyte microcapsule and the substrate.¹²³ Interestingly, beyond the threshold adhesion strength W_c , the contact length scale increases in proportion to $(W - W_c)^{1/2}$, which is the same as the behavior of vesicle adhesions except the coefficient before $(W - W_c)^{1/2}$.

6. A different viewpoint of surface tension

Although the lipid bilayer cannot withstand the in-plane shear strain, it can still endure the in-plane compression strain. The in-plane compression modulus, k_b , of lipid bilayers is about 0.24 N/m.¹²⁴ Considering this point, we may write the free energy of a closed lipid vesicle as

$$\mathcal{F} = p \int dV + \int G_B dA + \int (k_b/2)(2J_b)^2 dA, \quad (102)$$

where

$$G_B = (k_c/2)(2H + c_0)^2 - \bar{k}K, \quad (103)$$

and J_b is the in-plane compression or stretch strain. We emphasize that the contribution of chemical potential are omitted when we write the above free energy.

The first order variation of the free energy (102) reveals that $2J_b$ is a constant and then

$$p - 2(2k_b J_b)H + 2k_c \nabla^2 H + k_c(2H + c_0)(2H^2 - c_0H - 2K) = 0. \quad (104)$$

Comparing the above equation with the shape equation (77) of lipid vesicles, we deduce that

$$\lambda = 2k_b J_b. \quad (105)$$

In the discussion on the stability of closed lipid vesicles, we have seen that the surface tensor λ has no effect on the critical pressure. The second order variation of the free energy (102) can give the same conclusion. $\delta^2[p \int dV + \int G_B dA]$ has been shown in Eq. (82) with vanishing λ . The additional term is

$$\delta^2 \int (k_b/2)(2J_b)^2 dA = \int k_b(\text{div } \mathbf{v} - 2H\Omega_3)^2 dA \quad (106)$$

where $\mathbf{v} = \Omega_1 \mathbf{e}_1 + \Omega_2 \mathbf{e}_2 + \Omega_3 \mathbf{e}_3$ represents the infinitesimal displacement vector of the vesicle surface. We can always select the proper deformation modes such that $\text{div } \mathbf{v} - 2H\Omega_3 = 0$ and then $\delta^2 \int (k_b/2)(2J_b)^2 dA$ vanishes, but $\delta^2[p \int dV + \int G_B dA]$ is not affected. That is, the critical pressure is determined merely by $\delta^2[p \int dV + \int G_B dA]$, which is independent on the compression modulus of lipid bilayer k_b .

C. Cell membrane

Cell membrane consists of lipids, proteins, and a small quantity of carbohydrates and so on. A simple but widely accepted model for cell membranes is the fluid mosaic model¹²⁵ proposed by Singer and Nicolson in 1972. In this model, the cell membrane is considered as a lipid bilayer where the lipid molecules can move freely in the membrane surface like fluid, while the proteins are embedded in the lipid bilayer. Some proteins, so called integral membrane proteins, traverse entirely in the lipid bilayer and play the role of information and matter communications between the interior of the cell and its outer environment. The others, so called peripheral membrane proteins, are partially embedded in the bilayer and accomplish the other biological functions. Beneath the lipid membrane, the membrane skeleton, a network of proteins, links with the proteins embedded in the lipid membrane. Mature mammalian and human erythrocytes (i.e., red blood cells) are lack of a cell nucleus. Thus they provide a good experimental model for studying the mechanical properties of cell membranes.^{126,127,128,129} On the theoretical side, spontaneous curvature model,²⁹ rubber membrane model,^{30,130,131} and dual network model¹³² have been employed to investigate the mechanical and thermal fluctuation properties of erythrocyte membranes. We will address the elasticity and stability of composite shell model for cell membranes in this section.

1. Composite shell model of cell membranes

A cell membrane can be simplified as a composite shell¹³³ of lipid bilayer and membrane skeleton. The membrane skeleton, inside of the cell membrane, is a network of protein filaments as shown in Fig. 13. The joint points of the network are bulk proteins embedded in the lipid bilayer. The whole membrane skeleton seems to float the sea of the lipid bilayer. It can have a global movement along the surface of the bilayer but the movement of the joints along the normal direction is totally coupling with the bilayer. In the mechanical point of view, the lipid bilayer can endure the bending deformation but hardly bear the in-plane shear strain. On the contrary, the membrane skeleton can endure the in-plane shear strain but hardly bear the bending deformation. The composite shell overcomes the shortage of the lipid bilayer and the membrane skeleton. It can sustain both bending deformation and in-plane shear strain.

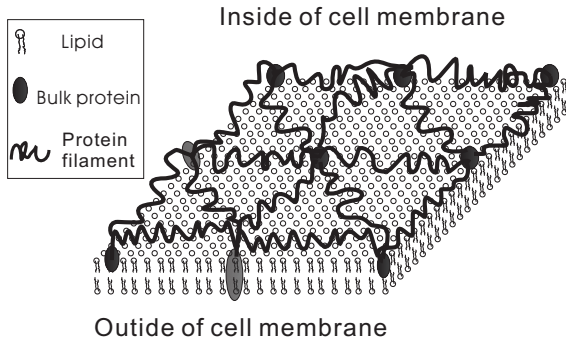


FIG. 13: Local schematic picture of the composite shell model for a cell membrane.

The contour length of protein chain between joints in the membrane skeleton is about 100 nm which is much smaller than the size ($\sim 10 \mu\text{m}$) of cell membranes. The lipid bilayer is 2D homogenous. The membrane skeleton is roughly a 2D locally hexagonal lattice. As is well known, the mechanical property of a 2D hexagonal lattice is 2D isotropic.¹³⁴ Thus the composite shell of the lipid bilayer plus the membrane skeleton can still be regarded as a 2D isotropic continuum. Its free energy density should be invariant under the in-plane coordinate transformation and can be written as $G_{cm} = G_{cm}(2H, K; 2J, Q)$. We can expand G_{cm} up to the second order terms of curvatures and strains as

$$G_{cm} = G_B + (k_b/2)(2J_b)^2 + G_{sk}, \quad (107)$$

where G_B results mainly from the bending energy of the lipid bilayer, which has the form as Eq. (103). $(k_b/2)(2J_b)^2$ is the contribution of in-plane compression of the lipid bilayer where k_b and $2J_b$ are the compression modulus and relative area compression of the lipid bilayer. $G_{sk} = (k_d/2)(2J)^2 - \tilde{k}Q$ is the in-plane compression and shear energy density which comes from the entropic elasticity of the membrane skeleton. k_d and \tilde{k}

are the compression and shear moduli of the membrane skeleton, respectively. Their values are experimentally determined as $k_d = \tilde{k} = 4.8 \mu\text{N/m}$.^{129,135} $2J$ and Q are the trace and determinant of the stain tensor of the membrane skeleton. Because there is no in-plane coupling between the lipid bilayer and the membrane skeleton in the composite shell model, thus J_b for the lipid bilayer and J for the membrane skeleton have no local correlation. In the above subsection, we have mentioned that the effect of $(k_b/2)(2J_b)^2$ can be replaced with the surface tension $\lambda = 2k_b J_b$. Considering a closed cell membrane under osmotic pressure p , the free energy can be written as

$$\mathcal{F} = \int G_{cm} dA + p \int dV. \quad (108)$$

Similarly to Sec. II C, if we define a displacement vector \mathbf{u} satisfying Eqs. (71) and (72), we can derive the Euler-Lagrange equations corresponding to the free energy (108) as

$$(\tilde{k} - 2k_d)\nabla(2J) - \tilde{k}(\diamond^2\mathbf{u} + K\bar{\mathbf{u}} + \tilde{\nabla}u_3) = 0, \quad (109)$$

$$p + 2k_c[(2H + c_0)(2H^2 - c_0H - 2K) + 2\nabla^2H] - 2\lambda H + 2H(\tilde{k} - k_d)(2J) - \tilde{k}\mathfrak{R} : \nabla\mathbf{u} = 0, \quad (110)$$

where $\bar{\mathbf{u}}$ and $\diamond^2\mathbf{u}$ are the in-plane components of \mathbf{u} and $\text{div}(\diamond\mathbf{u})$, respectively. \mathfrak{R} is the curvature tensor related to Eq. (5). $\tilde{\nabla}$ is called the gradient operator of the second class, which is shown in our previous work.⁴⁹

Generally speaking, it is difficult to find the analytical solutions to Eqs. (109) and (110). But we can verify that a spherical membrane with homogenous in-plane strains satisfy these equations. The radius R and the homogenous in-plane strain ε should obey the following relation:

$$pR^2 + 2(\lambda + 2k_d\varepsilon - \tilde{k}\varepsilon)R + k_c c_0(c_0R - 2) = 0. \quad (111)$$

2. Stability of cell membranes and the function of membrane skeleton

When the osmotic pressure is beyond some threshold, a closed cell membrane will lose its stability and change its shape abruptly. The threshold is called the critical pressure. To obtain it, one should calculate the second order variation of the free energy (108) in terms of Appendix B. The variational result is

$$\begin{aligned} \delta^2\mathcal{F} = & \int k_c[(\nabla^2\Omega_3)^2 + (2H + c_0)\nabla(2H\Omega_3) \cdot \nabla\Omega_3]dA \\ & + \int [4k_c(2H^2 - K)^2 + k_cK(c_0^2 - 4H^2) + 2\lambda K - 2Hp]\Omega_3^2dA \\ & + \int [k_c(14H^2 + 2c_0H - 4K - c_0^2/2) - \lambda]\Omega_3\nabla^2\Omega_3dA \\ & - 2k_c \int (2H + c_0)[\nabla\Omega_3 \cdot \tilde{\nabla}\Omega_3 + 2\Omega_3\nabla \cdot \tilde{\nabla}\Omega_3]dA \\ & - k_d \int [(\mathbf{v} \cdot \nabla + 2H\Omega_3)(\text{div}\mathbf{v} - 2H\Omega_3)]dA \\ & + (\tilde{k}/2) \int (\text{curl}\mathbf{v})^2dA - \tilde{k} \int K\bar{\mathbf{v}}^2dA + \tilde{k} \int \Omega_3\tilde{\nabla} \cdot \mathbf{v}dA \end{aligned}$$

$$+\tilde{k} \int 2H\Omega_3(\text{div } \mathbf{v} - 2H\Omega_3)dA - \tilde{k} \int \Omega_3 \mathfrak{R} : \nabla \mathbf{v} dA, \quad (112)$$

where $\mathbf{v} = \Omega_1 \mathbf{e}_1 + \Omega_2 \mathbf{e}_2 + \Omega_3 \mathbf{e}_3$ is the infinitesimal displacement vector of the cell membrane whose in-plane component is denoted as $\tilde{\mathbf{v}} = \Omega_1 \mathbf{e}_1 + \Omega_2 \mathbf{e}_2$.

In terms of the Hodge decomposed theorem,¹³⁶ \mathbf{v} can be expressed by two scalar functions Ω and χ as

$$\mathbf{v} \cdot d\mathbf{r} = d\Omega + *d\chi, \quad (113)$$

where $*$ is the Hodge star.^{49,136} Then we have $\text{div } \mathbf{v} = \nabla^2 \Omega$ and $\text{curl } \mathbf{v} = \nabla^2 \chi$. For the spherical cell membrane satisfying Eq. (111), Eq. (112) can be divided into two parts: one is

$$\delta^2 \mathcal{F}_1 = (\tilde{k}/2) \int [(\nabla^2 \chi)^2 + (2/R^2) \chi \nabla^2 \chi] dA; \quad (114)$$

another is

$$\begin{aligned} \delta^2 \mathcal{F}_2 = & \int \Omega_3^2 [2c_0 k_c / R^3 + p/R + (4k_d - 2\tilde{k})/R^2] dA \\ & + \int \Omega_3 \nabla^2 \Omega_3 [k_c c_0 / R + 2k_c / R^2 + pR/2] dA \\ & + \int k_c (\nabla^2 \Omega_3)^2 dA + [(4k_d - 2\tilde{k})/R] \int \Omega_3 \nabla^2 \Omega dA \\ & + k_d \int (\nabla^2 \Omega)^2 dA + (\tilde{k}/R^2) \int \Omega \nabla^2 \Omega dA. \end{aligned} \quad (115)$$

It is easy to verify that $\delta^2 \mathcal{F}_1$ is always positive on a spherical surface. Then the stability of the spherical cell membrane is merely determined by $\delta^2 \mathcal{F}_2$. By analogy with our previous work,¹³⁷ we can prove that $\delta^2 \mathcal{F}_2$ is also positive if

$$p < p_l \equiv \frac{2\tilde{k}(2k_d - \tilde{k})}{[k_d l(l+1) - \tilde{k}]R} + \frac{2k_c}{R^3} [l(l+1) - c_0 R], \quad (116)$$

for any integer $l \geq 2$. Thus the critical pressure is

$$p_c \equiv \min\{p_l \ (l = 2, 3, 4, \dots)\}. \quad (117)$$

Obviously, if $\tilde{k} = 0$, i.e., the effect of membrane skeleton vanishes in the cell membrane, p_c degenerates into the critical pressure (83) of a spherical lipid vesicle.

When $\tilde{k}k_d(2k_d - \tilde{k})R^2/k_c(6k_d - \tilde{k})^2 > 1$, the critical pressure is derived from Eqs. (116) and (117) as

$$p_c = (4/R^2) \sqrt{(\tilde{k}/k_d)(2k_d - \tilde{k})k_c}. \quad (118)$$

As an example, let us consider a cell membrane with typical values of $\tilde{k} = k_d = 4.8 \mu\text{N/m}$,¹²⁹ $k_c = 10^{-19} \text{ J}$, and $R \approx 10 \mu\text{m}$. Through a simply manipulation, we find that $\tilde{k}k_d(2k_d - \tilde{k})R^2/k_c(6k_d - \tilde{k})^2 \gg 1$, and so Eq. (118) holds, from which we obtain the critical pressure $p_c = 0.03 \text{ Pa}$. However, if the membrane skeleton vanishes, $\tilde{k} = 0$, we calculate $p_c = 0.001 \text{ Pa}$ from Eqs. (116) and (117). This example reveals a mechanical function of

membrane skeleton: it highly enhances the stability of cell membranes.

As a byproduct, Eq. (118) also gives the critical pressure

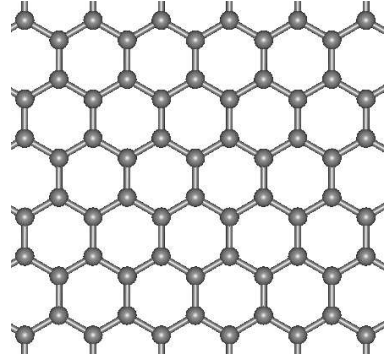
$$p_c = \sqrt{4/3(1-\nu^2)} Y(h/R)^2 \quad (119)$$

for a spherical thin solid shell of 3D isotropic materials if we take k_c , k_d , and \tilde{k} as Eqs. (63)–(65). This formula is the same as the classic strict result obtained by Pogorelov from the other method.¹³⁸

IV. APPLICATION OF ELASTIC THEORY IN NANO-STRUCTURES

In the last section, we have expatiated on the application of Elastic theory in bio-structures. In this section, we will discuss whether and to what extent this theory can be applied to nano-structures, especially the graphitic structures, such as graphene and carbon nanotubes.

(a)



(b)

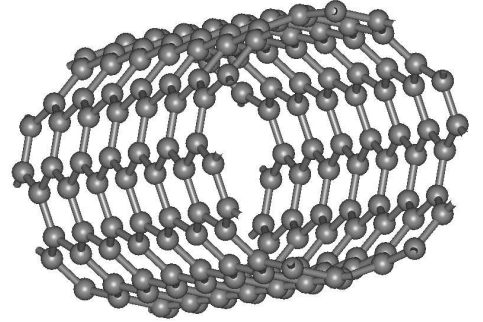


FIG. 14: (a) Graphene. (b) Single-walled carbon nanotube.

A. Graphene

Graphene is a single layer of carbon atoms with a 2D honeycomb lattice as shown in Fig. 14a. It has been a rapidly rising star in the material science and

condensed-matter physics¹³⁹ since it was successfully cleaved from buck graphite.¹⁴⁰ It is found that the free-standing graphene might be a strictly 2D atomic crystal which is stable under ambient conditions.¹⁴¹ However, Mermin has theoretically proved that the 2D crystalline order could not exist at finite temperature.¹⁴² There are two possible ways to solve this paradox: (i) The graphene might not be a perfect 2D crystal. Recently, Meyer *et al.* have investigated the elaborate structure of suspended graphene sheets and found that the graphene sheets are not genuine flat.¹⁴³ They also argue that the graphene sheets could be stabilized by the out-of-plane deformation in the third dimension resulting from the thermal fluctuations.¹⁴³ Fasolino *et al.* have also addressed the height fluctuations by means of Monte Carlo simulations.¹⁴⁴ Their result at room temperature is in good agreement with the experiment mentioned above. (ii) Mermin theorem is valid for power-law potentials of the Lennard-Jones type while the interaction between nearest neighbor atoms (covalent bond) in the graphene might not be of this type.¹⁴⁵

To fully understand the experimental result and possible stable mechanism in theory, we will address the Lenosky lattice model¹⁴⁶ and its revised form as follows.

1. Revised Lenosky lattice model and its continuum limit

We start from the concise formula proposed by Lenosky *et al.* in 1992 to describe the deformation energy of a single layer of curved graphite¹⁴⁶

$$E_g = \frac{\epsilon_0}{2} \sum_{(ij)} (r_{ij} - r_0)^2 + \epsilon_1 \sum_i \left(\sum_j \mathbf{u}_{ij} \right)^2 + \epsilon_2 \sum_{(ij)} (1 - \mathbf{n}_i \cdot \mathbf{n}_j) + \epsilon_3 \sum_{(ij)} (\mathbf{n}_i \cdot \mathbf{u}_{ij})(\mathbf{n}_j \cdot \mathbf{u}_{ji}). \quad (120)$$

The first two terms are the contributions of bond length and bond angle changes to the energy. The last two terms are the contributions from the π -electron resonance. In the first term, r_0 is the initial bond length of planar graphite, and r_{ij} is the bond length between atoms i and j after the deformations. In the remaining terms, \mathbf{u}_{ij} is a unit vector pointing from atom i to its neighbor j , and \mathbf{n}_i is the unit vector normal to the plane determined by the three neighbors of atom i . The summation $\sum_{(j)}$ is taken over the three nearest neighbor atoms j to atom i , and $\sum_{(ij)}$ taken over all the nearest neighbor atoms. The parameters $(\epsilon_1, \epsilon_2, \epsilon_3) = (0.96, 1.29, 0.05)$ eV were determined by Lenosky *et al.*¹⁴⁶ through local density approximation. The value of ϵ_0 was given by Zhou *et al.* as $\epsilon_0 = 57$ eV/Å² through the force-constant method.¹⁴⁷

In the above energy form, the second term requires that the energy cost due to in-plane bond angle changes is the same as that due to out-of-plane bond angle changes. However, the experiment by inelastic neutron scattering techniques reveals that the energy costs due to in-plane and out-of plane bond angle changes are quite different

from each other.¹⁴⁸ To describe this effect, we revise the Lenosky lattice model as

$$E_g = \frac{\epsilon_0}{2} \sum_{(ij)} (r_{ij} - r_0)^2 + \epsilon_{1t} \sum_i \sum_{(j<k)} (\mathbf{u}_{ij}^t \cdot \mathbf{u}_{ik}^t + 1/2)^2 + \epsilon_{1n} \sum_i \left(\sum_j \mathbf{u}_{ij}^n \right)^2 + \epsilon_2 \sum_{(ij)} (1 - \mathbf{n}_i \cdot \mathbf{n}_j), \quad (121)$$

where $\mathbf{u}_{ij}^t = \mathbf{u}_{ij} - (\mathbf{n}_i \cdot \mathbf{u}_{ij})\mathbf{n}_i$ and $\mathbf{u}_{ij}^n = \mathbf{n}_i \cdot \mathbf{u}_{ij}$. If the three nearest neighbor atoms to atom i are labeled as 1,2,3, the summation $\sum_{(j<k)}$ is understood as $\sum_{1 \leq j < k \leq 3}$. The second and third terms of Eq. (121) represent the energy costs due to in-plane and out-of-plane bond angle changes, respectively. We have omitted the term $\epsilon_3 \sum_{(ij)} (\mathbf{n}_i \cdot \mathbf{u}_{ij})(\mathbf{n}_j \cdot \mathbf{u}_{ji})$ relative to the original Lenosky model (120), because its contribution is very small in terms of the results by Lenosky *et al.*

The parameters in Eq. (121) are determined by fitting the total energy of variously perturbed configurations of $\sqrt{7} \times \sqrt{7}$ unit cell of graphite (14 atoms). The total energy is obtained through the first-principles calculations (the ABINIT package¹⁴⁹). The calculations are carried by taking Troullier-Martins pseudopotentials,¹⁵⁰ plane-wave energy cutoff of 50 Hartree, and $4 \times 4 \times 1$ Monkhorst-Pack k-points¹⁵¹ in Brillouin-zone. The exchange-correlation energy are treated within the local-density approximation in the Ceperley-Alder form¹⁵² with the Perdew-Wang parametrization.¹⁵³ Our result is $r_0 = 1.41$ Å, $\epsilon_0 = 46.34$ eV/Å², $\epsilon_{1t} = 4.48$ eV, $\epsilon_{1n} = 1.04$ eV, and $\epsilon_2 = 1.24$ eV. The value of ϵ_0 is a little smaller than that obtained by Zhou *et al.*¹⁴⁷ from force constant method. The values of ϵ_{1n} and ϵ_2 are very close to those of ϵ_1 and ϵ_2 obtained by Lenosky *et al.*¹⁴⁶ from local density approximation. The key reason is that the main energy contribution in the configurations discussed by Lenosky *et al.* comes from the third and fourth term in Eq. (121).

Now let us derive the continuum limit form of the revised Lenosky lattice model (121) by analogy with the method in our previous work.^{42,44} Now consider a curved graphene and take a fictitious smooth surface such that all carbon atoms are on that surface. The in-plane strain can be expressed as $\mathfrak{E}_i = \begin{pmatrix} \epsilon_{11} & \epsilon_{12} \\ \epsilon_{12} & \epsilon_{22} \end{pmatrix}$ in the local frame $\{\mathbf{e}_1, \mathbf{e}_2, \mathbf{e}_3\}$ at atom i . The bond vector \mathbf{r}_{ij} from atom i to its neighbor j after the deformations and the initial bond vector \mathbf{r}_{ij}^0 before the deformations satisfy $\mathbf{r}_{ij} = (\mathbf{I} + \mathfrak{E}_i) \cdot \mathbf{r}_{ij}^0$, where \mathbf{I} is the unit matrix. The initial bond vectors \mathbf{r}_{ij}^0 can be expanded to the order of $O(r_0^2 \kappa^2)$ as⁴⁷

$$\mathbf{r}_{ij}^0 = (1 - r_0^2 \kappa_j^2 / 6) r_0 \mathbf{T}_j + (\kappa_j \tau_j r_0^3 / 6) \mathbf{B}_j + [r_0 \kappa_j / 2 + (r_0^2 / 6) d\kappa_j / ds] r_0 \mathbf{N}_j, \quad (122)$$

where $j=1, 2, 3$ denote three sp^2 -bond curves from atom i to one of its three neighbor atoms j on the graphene surface. The symbols \mathbf{T}_j , \mathbf{N}_j , and \mathbf{B}_j represent the unit tangential, normal, and binormal vectors of the bond curve

from i -atom to j -atom, which satisfy the Frenet theorem Eq. (1). κ, τ refer to the curvature and torsion while s is the arc-length parameter along the bond curve. Assume the sp^2 -bond along the geodesic curve of the graphene surface. The vectors \mathbf{T}_j and \mathbf{B}_j can be expressed by $\mathbf{T}_j = \cos\theta_j\mathbf{e}_1 + \sin\theta_j\mathbf{e}_2$ and $\mathbf{B}_j = -\sin\theta_j\mathbf{e}_1 + \cos\theta_j\mathbf{e}_2$, where θ_j is the rotating angle from \mathbf{e}_1 to \mathbf{T}_j . We have the expressions of $\mathbf{u}_{ij} = \mathbf{r}_{ij}/r_{ij}$ and $\mathbf{n}_i = \mathbf{N}_j$ with $r_{ij} = |\mathbf{r}_{ij}|$ for the deformed graphene. Then Eq. (121) is transformed into the continuum limit up to the second-order magnitudes of $\varepsilon_{11}, \varepsilon_{22}, \varepsilon_{12}$ and $r_0\kappa$ as

$$E_g = \int \left[\frac{k_c}{2}(2H)^2 - \bar{k}K + \frac{k_d}{2}(2J)^2 - \tilde{k}Q \right] dA, \quad (123)$$

with four parameters

$$k_c = (9\epsilon_{1n} + 6\epsilon_2)r_0^2/8\Omega_0, \quad (124)$$

$$\bar{k} = 3\epsilon_2r_0^2/4\Omega_0, \quad (125)$$

$$k_d = 9(\epsilon_0r_0^2 + 3\epsilon_{1t})/16\Omega_0, \quad (126)$$

$$\tilde{k} = 3(\epsilon_0r_0^2 + 9\epsilon_{1t})/8\Omega_0, \quad (127)$$

where $\Omega_0 = 3\sqrt{3}r_0^2/4$ is the occupied area per atom. The continuum form (123) has first derived in our previous work 44 which is, in fact, the natural conclusion of the symmetry of graphene.¹⁵⁴ The curved graphene comprises a lot of hexagons which has approximately local hexagonal symmetry. In fact, 2D structures with hexagonal symmetry are 2D isotropic.¹³⁴ Thus the elasticity of the graphene can be reasonably described by the shell theory of 2D isotropic materials mentioned in Sec. II C and so its energy has the form of Eq. (123). We also notice that a flaw in the coefficient before ϵ_1 in the expression of k_c in our previous work 44.

Using the values of $r_0, \epsilon_{1t}, \epsilon_{1n}$, and ϵ_2 obtained from the first-principles calculations, we have $k_c = 1.62$ eV, $\bar{k} = 0.72$ eV, $k_d = 22.97$ eV/Å², and $\tilde{k} = 19.19$ eV/Å². Because the results of first-principles calculation are applicable for zero temperature, only the results derived from the experiments at low temperature can be used as reference values to compared with them. The value of k_c is close to the value 1.77 eV estimated by Komatsu^{155,156,157} at low temperature (less than 60 K). The value $\tilde{k}/k_d = 0.83$ is quite close to the experimental value 0.8 derived from the in-plane elastic constants of graphite.¹⁵⁸ The elastic properties of graphene can be described by Eq. (123) with four parameters k_c, \bar{k}, k_d , and \tilde{k} , where the energy density is the same as Eq. (62), the free energy density of solid shell with 2D isotropic materials. Since $\bar{k}/k_c = 0.44$ is much smaller than $\tilde{k}/k_d = 0.83$, the graphene cannot be regarded as a solid shell with 3D isotropic materials as Ref. 44.

2. Intrinsic roughening in graphene at temperature T

Let us consider the freely suspended graphene which is almost a flat layer with the area L^2 . The small out-of-plane displacement is denoted by w . The energy (123) is

transformed into

$$E_g = (k_c/2) \int (\nabla^2 w)^2 d^2\mathbf{x}, \quad (128)$$

where $\mathbf{x} \equiv (x_1, x_2)$ represents the point on the graphene plane before deformations.

Adopting the Fourier series

$$w(\mathbf{x}) = (1/L) \sum_{\mathbf{q}} \tilde{w}_{\mathbf{q}} \exp\{i\mathbf{q} \cdot \mathbf{x}\}, \quad (129)$$

with $\mathbf{q} \equiv (2l\pi/L, 2n\pi/L)$, we transform Eq. (128) into

$$E_g = (k_c/2) \sum_{\mathbf{q}} \mathbf{q}^4 |\tilde{w}_{\mathbf{q}}|^2, \quad (130)$$

and then the corresponding partition function is derived as

$$\mathcal{Z} = \int \prod_{\mathbf{q}} d\tilde{w}_{\mathbf{q}} \exp(-E_g/T) = \prod_{\mathbf{q}} \sqrt{2\pi T/k_c \mathbf{q}^4}, \quad (131)$$

where the Boltzmann constant has been set to 1. It follows that the equipartition theorem:

$$\langle (k_c/2) \mathbf{q}^4 |\tilde{w}_{\mathbf{q}}|^2 \rangle = -T \partial \ln \mathcal{Z} / \partial \ln \mathbf{q}^4 = T/2, \quad (132)$$

where $\langle \cdot \rangle$ represents the ensemble average. The above equation is equivalent to

$$\langle |\tilde{w}_{\mathbf{q}}|^2 \rangle = T/k_c \mathbf{q}^4. \quad (133)$$

Similarly, $\langle w^2 \rangle$ is derived as

$$\langle w^2 \rangle = \sum_{\mathbf{q}} \frac{\langle |\tilde{w}_{\mathbf{q}}|^2 \rangle}{L^2} = \frac{TL^2}{16\pi^4 k_c} \sum_{ln} \frac{1}{(l^2 + n^2)^2}. \quad (134)$$

Through simply numerical manipulations, we have¹⁵⁹

$$\langle w^2 \rangle \simeq \frac{TL^2}{150k_c}, \quad (135)$$

for the graphene contains more than 100 atoms.

In terms of Ref. 157, we estimate $k_c \approx 0.46$ eV at $T = 300$ K. Substituting it into Eq. (135) and taking $L = 25$ nm as the experiment 143, we have $\sqrt{\langle w^2 \rangle} \approx 0.5$ nm. This value is a little smaller than the largest out-of-plane deformation 1 nm in the experiment. However, they are consistent with each other because 0.5 nm is the mean square value which should be smaller than the largest out-of-plane deformation in the experiment.

B. Carbon nanotube

There are two kinds of carbon nanotubes: single- and multi-walled carbon nanotubes, which are synthesized in the last decade of 20 century.^{160,161} Simply speaking, a single-walled carbon nanotube (SWNT) can be regarded

as a seamless cylinder wrapped up from a graphitic sheet, as shown in Fig. 14b, whose diameter is in nanometer scale and length from tens of nanometers to several micrometers if we ignore its two end caps. A multi-walled carbon nanotube (MWNT) consists of a series of coaxial SWNTs with layer distance about 3.4 Å.

SWNTs can be expressed as a pair of integers (n,m) , so called index, in terms of the wrapping rule. They are divided into two classes: achiral tubes if $n = m$ or $nm = 0$ and chiral tubes for others.¹⁶² The electronic properties of SWNTs depend sensitively on the index:¹⁶³ they are metallic if $n - m$ is multiple of 3, else semiconductor. SWNTs also possess many novel mechanical properties,¹⁶⁴ in particular high stiffness and axial strength, which are not sensitive to the tube diameters and chirality. MWNTs have the similar mechanical properties to SWNTs.^{165,166} In this section, we will review the theoretical and numerical results on the elastic properties of carbon nanotubes, and then discuss how the low-dimensional elastic theory mentioned in Sec. II can be applied in carbon nanotubes.

1. General review on the elasticity of carbon nanotubes

The early researches on the elasticity of carbon nanotubes are focused on their Young's modulus Y and Poisson ratio ν . A SWNT is a single layer of carbon atoms. What is the thickness h of the atomic layer? It is a widely controversial question. Three typical values of the thickness listed in Table I are adopted or obtained in the previous literature Refs. 40, 41, 44 and 167–180. The first one is about 0.7 Å obtained from fitting the atomic scale model with the elastic shell theory of 3D isotropic materials.^{167,168,169,170,171,172,173} The second one is about 1.4 Å derived from molecular dynamics or finite element method.^{174,175} The third one is about 3.4 Å adopting the layer distance of bulk graphite.^{176,177,178,179,180} Recently, Huang *et al.* have investigated the effective thickness of SWNTs and found it depends on the type of loadings.¹⁸¹

The size- or chirality-dependent elastic properties of SWNTs have also been discussed by molecular mechanics model^{182,183,184} and *ab initio* calculations.^{173,185} The common conclusion is that the Young's modulus and Poisson ratio depend weakly on the diameter and chirality of SWNTs if the diameter is larger than 1 nm. Only for very small SWNTs, the size and chirality effect is evident. The SWNTs synthesized in the laboratory have usually the diameters larger than 1 nm; thus the size and chirality effect can be neglected safely.

The axial tension properties of MWNTs depend on the layer number of MWNTs for the small layer number and approach quickly to the properties similar to the bulk graphite.^{44,186,187}

The buckling and stability of carbon nanotubes under pressure or bending is a hot topic in the recent researches, where the critical pressure, moment or the equivalent quantity, critical strain, are highly concerned. A long

TABLE I: Young's modulus Y (unit in TPa), Poisson ratio ν and effective thickness h (unit in Å). (MD = molecular dynamics; TB = tight-binding; SM = structure mechanics; FEM = finite element method; LDA = local density approach)

Authors	Y	ν	h	Method	Refs.
Yakobson <i>et al.</i>	5.5	0.19	0.66	MD	40
Tu & Ou-Yang	4.7	0.34	0.75	LDA	44
Kudin <i>et al.</i>	3.9	0.15	0.89	<i>ab initio</i>	167
Zhou <i>et al.</i>	5.1	0.24	0.74	TB	168
Vodenitcharova <i>et al.</i>	4.9	–	0.62	ring theory	169
Pantano <i>et al.</i>	4.8	0.19	0.75	SM & FEM	170,171
Chen and Cao	6.8	–	0.80	SM	172
Wang <i>et al.</i>	5.1	0.16	0.67	<i>ab initio</i>	173
Sears & Batra	2.5	0.21	1.34	MD	174
Tserpes <i>et al.</i>	2.4	–	1.47	FEM	175
Lu	1.0	0.28	3.4	MD	41
Hernandez <i>et al.</i>	1.2	0.18	3.4	TB	176
Shen & Li	1.1	0.16	3.4	force-field	177
Li & Chou	1.0	–	3.4	SM	178
Bao <i>et al.</i>	0.9	–	3.4	MD	179
Zhou <i>et al.</i>	0.8	0.32	3.4	LDA	180

enough carbon nanotube under an axial loading might be regarded as a Euler rod and the axially critical strain is³

$$\varepsilon_{zc}^{rod} = \alpha\pi^2\mathcal{I}/AL^2 \propto (\rho/L)^2, \quad (136)$$

where L , ρ and A are the length, radius and cross-sectional area of the carbon nanotube, respectively. \mathcal{I} is the moment of inertia of the nanotube. The value of α depends on the boundary conditions of the carbon nanotube. This relation has been investigated by atomic-scale finite element method^{188,189,190} and molecular dynamics method or *ab initio* calculations.^{191,192,193,194,195} The basic numerical result is that the tube exhibits rod-like buckling behavior as the right-handed side of Eq. (136) if $L \gg \rho$. The Timoshenko beam theory, a more complicated theory than Euler rod theory, is also employed to discuss the buckling of MWNTs.¹⁹⁶ The difference between the results of both theories vanishes for large value of L/ρ .

For a short carbon nanotube under axial loading, the continuous shell model of 3D isotropic materials are widely used.^{40,188,189,190,192,193,194,197,198,199} The axially critical strain of a short SWNT is¹³⁸

$$\varepsilon_{zc}^{shell} = [\alpha/\sqrt{3(1-\nu^2)}](h/\rho) \propto \rho^{-1}, \quad (137)$$

where ρ and h are the radius and effective thickness of the SWNT, respectively. ν is the Poisson ratio of the SWNT. The value of α depends on the boundary condition of the carbon nanotube. For a short MWNT, the above relation is applicable for the outmost layer of the tube because the inter-layer interaction of

MWNTs is very small.²⁰⁰ It has also been investigated by atomic-scale finite element method,^{188,189,190,198} molecular dynamics method,^{40,192,193,194,199} and nanoindent experiment.^{201,202} It is found that the tube displays indeed the shell-like buckling behavior as the right-handed side of Eq. (137) for the tube aspect ratio $L/\rho < 10$.

The stability of a long SWNT under radial hydrostatic pressure might also be described by the continuous shell model of 3D isotropic materials, and the critical pressure is¹³⁸

$$p_{cr}^{shell} \propto \rho^{-3}, \quad (138)$$

where ρ is the radius of the SWNT. This relation has recently been confirmed by Hasegawa and Nishidate²⁰³ through *ab initio* calculations. The stability of a MWNT under radial hydrostatic pressure might also have the similar relation as Eq. (138) if only we take ρ as the outmost radius of the MWNT, because the transverse elasticity of MWNTs^{204,205} is much weaker than the in-plane elasticity of the outmost single layer of tube.

Bending can also result in the buckling of SWNTs. The kink phenomenon in a SWNT under pure bending has been investigated through molecular dynamics simulations and finite element method.^{40,206} The critical curvature can be described as

$$\kappa_{cr} = \varepsilon_{zc}^{shell} / \rho \propto \rho^{-2}, \quad (139)$$

where ρ is the radius of the SWNT. The kink phenomenon in a MWNT under pure bending satisfies the similar relation to Eq. (139) with small correction due to inter-layer van de Waals interactions^{207,208,209} if only we take ρ as the outmost radius of the MWNT.

Here we would not further discuss the problems on the buckling of MWNTs embedded in an elastic medium,^{210,211,212,213,214,215} the post-buckling behavior and the plastic properties of carbon nanotubes,^{216,217,218,219,220,221,222} as well as the mechanical properties of nanotube composites,^{223,224,225,226,227,228} rather than recommend gentle readers to consult the corresponding literature.

2. What are the fundamental quantities for SWNTs?

As mentioned above, different thickness leads to different Young's modulus (see Table I), which implies that the Young's modulus and thickness of SWNTs are not well-defined physical quantities.²²⁹ However, the in-plane Young's modulus $Y_s = Yh$ has the similar value $22 \text{ eV}/\text{\AA}^2$. Thus it is a more well-defined quantity than the Young's modulus and the thickness. Here we may ask: what are the fundamental quantities for SWNTs?

A SWNT is also a single layer of graphite, whose deformation energy can be also described as the revised Lenosky model (121). The corresponding continuum limit is Eq. (123) which contains four elastic constants

k_c , \bar{k} , k_d , and \tilde{k} . These four quantities avoid the controversial thickness of SWNTs. We suggest to use them as the fundamental quantities for SWNTs from which we can obtain some reduced quantities as follows.

Let us consider a cylinder under an axial loading with line density f along the circumference. The corresponding axial and circumferential strains are denoted as ε_{11} and ε_{22} . With Eq. (123), the free energy of this system is written as

$$\mathcal{F} \approx 2\pi\rho L[(k_d/2)(\varepsilon_{11} + \varepsilon_{22})^2 - \tilde{k}\varepsilon_{11}\varepsilon_{22} - f\varepsilon_{11}] \quad (140)$$

where L and ρ are the length and radius of the SWNT. The in-plane Young's modulus and Poisson ratio can be defined as $Y_s = f/\varepsilon_{11}$ and $\nu_s = -\varepsilon_{22}/\varepsilon_{11}$. From $\partial\mathcal{F}/\varepsilon_{11} = 0$ and $\partial\mathcal{F}/\varepsilon_{22} = 0$, we derive

$$Y_s = \tilde{k}(2 - \tilde{k}/k_d) = 22.35 \text{ eV}/\text{\AA}^2, \quad (141)$$

$$\nu_s = 1 - \tilde{k}/k_d = 0.165, \quad (142)$$

where the value of Y_s is close to the in-plane Young's modulus derived from Table I. It is in between 20 – $23 \text{ eV}/\text{\AA}^2$ obtained by Sánchez-Portal *et al.*²³⁰ It is much larger than the value $15 \text{ eV}/\text{\AA}^2$ obtained by Arroyo *et al.*²³¹ and Zhang *et al.*,²³² and $17 \text{ eV}/\text{\AA}^2$ by Caillerie *et al.*,²³³ but smaller than $34.6 \text{ eV}/\text{\AA}^2$ for armchair tube by Wang.²³⁴ The value of ν_s is close to the value 0.16 – 0.19 obtained by Yakobson *et al.*,⁴⁰ Kudin *et al.*,¹⁶⁷ Pantano *et al.*,^{170,171} Wang *et al.*,¹⁷³ Hernandez *et al.*,¹⁷⁶ and Shen *et al.*¹⁷⁷

The other quantity, the bending rigidity D , is also widely discussed in literature. In terms of Eq. (123), the energy per area of a SWNT without the in-plane strains can be expressed as

$$G_g = k_c/2\rho^2 \equiv D/2\rho^2. \quad (143)$$

Thus the bending rigidity

$$D = k_c = 1.62 \text{ eV}, \quad (144)$$

which is quite close to the value 1.49 – 1.72 eV obtained by Kudin *et al.*¹⁶⁷ and Sánchez-Portal *et al.*²³⁰ through *ab initio* calculations. It is a little larger than the values 0.85 – 1.22 eV obtained by Yakobson *et al.*,⁴⁰ Pantano *et al.*,^{170,171} and Wang.²³⁴

In terms of Eqs. (141)–(144), we can infer the values of k_d , \tilde{k} , k_c from the previous literature, which are listed in Table II. There is still lack of literature on \tilde{k} except our previous work^{42,44,154} and the present review. More work on \tilde{k} would be highly appreciated in the future.

We should emphasize that our formula (123) holds approximate up to the order of $(r_0/\rho)^2$ for SWNTs, where r_0 is the C-C length and ρ the radius of the SWNT. The omitted terms is in the order of $(r_0/\rho)^4$. This is the main reason for the size effect on the elastic constants in the very small SWNTs found in Refs. 173,182,183,184,185. Additionally, we have not considered the effect of Stone-Wales defects on the local properties of carbon nanotubes. In terms of Refs. 235 and 236, we can deduce that the defects reduce the the elastic constants of carbon nanotubes.

TABLE II: The values of Y_s , ν_s , k_d , \tilde{k} , k_c and \bar{k} . (MD = molecular dynamics; TB = tight-binding; SM = structure mechanics; FEM = finite element method; LDA = local density approach; CTIP=continuum theory of interatomic potential)

Authors	Y_s (eV/Å ²)	ν_s	k_d (eV/Å ²)	\tilde{k} (eV/Å ²)	k_c (eV)	\bar{k} (eV)	Method	Refs.
Yakobson <i>et al.</i>	22.69	0.19	23.54	19.06	0.85	–	MD	40
Tu & Ou-Yang	22.03	0.34	24.88	16.44	1.17	0.75	LDA	44
Tu & Ou-Yang	21.63	0.18	22.35	18.33	1.30	0.88	LDA	154
Kudin <i>et al.</i>	21.69	0.15	22.19	18.86	1.49–1.53	–	<i>ab initio</i>	167
Zhou <i>et al.</i>	23.59	0.24	25.03	19.02	1.14	–	TB	168
Pantano <i>et al.</i>	22.5	0.19	23.34	18.91	1.09	–	SM & FEM	170,171
Chen and Cao	34.38	–	–	–	–	–	SM	172
Wang <i>et al.</i>	21.36	0.16	21.92	18.41	0.82	–	<i>ab initio</i>	173
Sears & Batra	20.94	0.21	21.90	17.30	3.28	–	MD	174
Tserpes <i>et al.</i>	22.05	–	–	–	–	–	FEM	175
Lu	21.25	0.28	23.06	16.60	–	–	MD	41
Hernandez <i>et al.</i>	25.50	0.18	26.35	21.61	–	–	TB	176
Shen & Li	23.38	0.16	23.99	20.16	–	–	force-field	177
Li & Chou	21.25	–	–	–	–	–	SM	178
Bao <i>et al.</i>	19.13	–	–	–	–	–	MD	179
Zhou <i>et al.</i>	17.00	0.32	18.94	12.88	–	–	LDA	180
Sánchez-Portal	19.41–22.40	0.12–0.19	19.92–23.00	16.73–19.31	1.49–1.72	–	<i>ab initio</i>	230
Arroyo <i>et al.</i>	15.19	0.40	18.08	10.85	0.69	–	FEM	231
Zhang <i>et al.</i>	14.75	–	–	–	–	–	CTIP	232
Caillerie <i>et al.</i>	17.31	0.26	18.57	13.74	–	–	CTIP	233
Wang	34.63 or 17.31	–	–	–	1.12 or 1.21	–	CTIP	234
Present work	22.35	0.16	22.97	19.19	1.62	0.72	LDA	–

3. Revisit the stability of SWNTs

Now we will revisit the stability of SWNTs with the four fundamental quantities k_c , \tilde{k} , k_d , and \bar{k} or the corresponding reduced quantities.

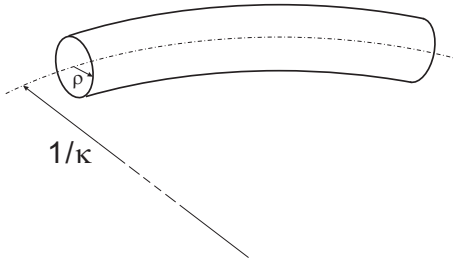


FIG. 15: Bent SWNT. ρ and $1/\kappa$ are the radii of the SWNT and the centerline of the SWNT, respectively.

First, let us consider a bent SWNT as shown in Fig. 15 where ρ and $1/\kappa$ are the radii of the SWNT and the centerline of the SWNT, respectively. Assume that the centerline of the SWNT is not extended and the cross section of the SWNT is still flat after bending under the condition $\rho \ll L \ll 1/\kappa$, where L is the total length of the centerline. In terms of Eq. (123), we can derive the

deformation energy due to bending as

$$\Delta\mathcal{F} \approx \int_0^L (k_{rod}/2)\kappa^2 ds, \quad (145)$$

where ds is the arc length element of the centerline. The bending modulus of the rod is $k_{rod} = \pi\rho[(2 - \tilde{k}/k_d)\tilde{k}\rho^2 + k_c]$. For the SWNT with diameter in the order of 1 nm, we can estimate $k_c \ll (2 - \tilde{k}/k_d)\tilde{k}\rho^2$. Considering Eq. (141), we have

$$k_{rod} \approx \pi Y_s \rho^3. \quad (146)$$

If an axial compression force F is loaded on the both ends of the SWNT, following Euler rod theory,² we can easily derive the critical force, above which the SWNT is unstable, as

$$F_c^{rod} = 2\alpha\pi k_{rod}/L^2, \quad (147)$$

where α depends on the boundary conditions in two ends of the SWNT. Defining the critical strain as $\varepsilon_{zc}^{rod} = F_c^{rod}/2\pi\rho Y_s$ and considering the above two equations, we can derive

$$\varepsilon_{zc}^{rod} = \alpha(\rho/L)^2. \quad (148)$$

This relation has the same asymptotic behavior as Eq. (136), which, as mentioned above, has been confirmed by a lot of theoretical and numerical researches.

Secondly, let us consider a short SWNT with radius ρ and an axial compression force loaded on its two ends. The force per length along the circumference is denoted as f . Following Ru's work,¹⁹⁷ considering Eq. (123) we have the critical axial force density as

$$f_c^{shell} = \alpha \sqrt{k_c Y_s} / \rho, \quad (149)$$

and the corresponding critical strain

$$\varepsilon_{zc}^{shell} \equiv f_c / Y_s = (\alpha / \rho) \sqrt{k_c / Y_s}, \quad (150)$$

where α depends on the boundary conditions in two ends of the SWNT. Y_s is the in-plane Young's modulus as shown in Eq. (141). The above relation (150) has the same asymptotic behavior as Eq. (137), which, as mentioned in above, has been confirmed by several theoretical and numerical researches.

Thirdly, let us consider a long enough SWNT with radius ρ and a radial compression pressure p loaded on its surface. In terms of the similar method on the stability of cell membranes, we can derive the critical pressure

$$p_{cr}^{shell} = 3k_c / \rho^3, \quad (151)$$

above which the SWNT will lose its stability. This relation has the same asymptotic behavior as Eq. (138). The corresponding critical circumferential strain is

$$\varepsilon_c^{cir} = 2\rho p_{cr}^{shell} / Y_s = 6k_c / Y_s \rho^2. \quad (152)$$

Comparing Eq. (151) with (85), one can find that the critical pressures for carbon nanotubes and lipid tubules are in the same form. Yin *et al.* have noticed this similarity in the recent work²³⁷. However, the profound mechanism is different: nanotubes can endure the shear strain while lipid tubules cannot.

It seems that no literature discusses the possible instability of a SWNT under axial tension. Here we will give a qualitative analysis. Assume the tension density (i.e., force per length) to be f . The axial strain under the tension is f / Y_s and the corresponding circumferential strain is $\nu_s f / Y_s$. When it is beyond the critical value (152), the SWNT will be instable. Thus we obtain the critical tension density

$$f_c^{tsn} = 6k_c / \nu_s \rho^2. \quad (153)$$

Only if f_c^{tsn} is below the strength of the SWNT, the buckling phenomenon under tension can be observed.

Till now, we have not found that \bar{k} exists explicitly in the above equations (148)–(152) for nanotubes. Because the term related to \bar{k} in the free energy (123) can be transformed into the boundary term with the aid of Gauss-Bonnet formula, \bar{k} should be implicitly contained by α in these equations, which need the further investigations in the future.

V. CONCLUSION AND PROSPECT

In summary, we present the elastic theory of low-dimensional (one- and two-dimensional) continua and its applications in bio- and nano-structures. The elastic theory of Kirchhoff rod, Helfrich rod, bending-soften rod, fluid membrane, and solid shell is revisited. We construct the free energy density of the continua on the basis of the symmetry argument. The fundamental equations can be derived from the bottom-up and the top-down standpoints. Although they have different forms obtained from these two viewpoints, several examples reveal that they are, in fact, equivalent to each other. We investigate the kink stability of short DNA rings, the elasticity of lipid membranes, and the adhesions between a vesicle and a substrate or another vesicle. A cell membrane is simplified as a composite shell of lipid bilayer and membrane skeleton. The membrane skeleton is shown to enhance highly the mechanical stability of cell membranes. We propose a revised Lenosky lattice model based on the local density approximation and derive its continuum form up to the second order terms of curvatures and strains, which is the same as the free energy of 2D solid shells. The intrinsic roughening of graphene and several typical mechanical properties of carbon nanotubes are addressed by using this continuum form. We can abandon the controversial thickness and Young's modulus of graphene and SWNTs if we adopt this continuum form to describe the mechanical properties of graphene and SWNTs.

Finally, we would like to list a few open problems which need to be addressed in the future work.

(i) The vesicles with lipid domains have been investigated in Sec. III B. There is a special lipid domain at liquid-ordered phase, so called the raft, which is enriched in cholesterol and sphingolipids. Cholesterol is a kind of chiral lipid molecules, which has not been included in the previous and present theory of lipid domains. A new theory with the chirality on the raft domain should be developed.

(ii) The composite shell, as a model of cell membranes, has been investigated in Sec. III C where the constraint between the area of the lipid bilayer and membrane skeleton is totally neglected. Additionally, only the small deformation of cell membranes are addressed in this review. The large deformation behavior of cell membranes^{238,239,240} has recently discussed through numerical simulations. It is necessary to reconsider the composite shell model with the constraint $\int J dA = \int J_b dA$ and its behavior under large deformation theoretically.

(iii) We suggest adopting four parameters k_c , \bar{k} , k_d , and \bar{k} to describe the mechanics of graphitic structures in Sec. IV. However, there are sparse studies on \bar{k} in previous literature. It is highly expected to theoretical and experimental work on this quantity.

(iv) We only talk about the thermal fluctuation on the discussion of graphene. The fluctuations of DNA, lipid

membranes, and cell membranes are not in the range of our topics, on which we suggest that gentle readers consult Refs.10,33,63,64.

(v) The elastic theory presented in this review is a static theory. Thus we are very regretted that we have to omit several important subjects such as the vesicles in shear flows,^{241,242,243,244,245} and dynamic response of carbon nanotubes or nanotube networks^{246,247} and so on. These topics will be quickly developed in the future.

Acknowledgements

We are very grateful to Dr. Q. X. Li and Prof. T. Lenosky for their help in our DFT calculations. We thank Prof. G.-L. Xu because he let us know the work by Giaquinta and Hildebrandt, which we have not noticed before. We are grateful to Prof. Z.-C. Zhou for his kind comments. Some materials in this review are prepared in Tamkang University where ZCT is supported by the National Science Council (grant no. NSC 94-2119-M-032-010), and the others are prepared in Universität Stuttgart where ZCT is supported by the Alexander von Humboldt foundation. ZCT is also grateful to the support of Nature Science Foundation of China (grant no. 10704009).

Note added in proof

After this review was in press, we noticed that recent researches^{248,249} on the mechanical properties of nanosprings²⁴⁸ and amorphous straight nanowires²⁴⁹ within the framework of Kirchhoff rod. We were also informed of the researches^{250,251} by Arroyo and Belytschko on discussing the buckling pattern of multi-walled carbon nanotubes under pure bending. Additionally, we emphasize that the similar equations to (114) and (115) without p first obtained by Zhang et al.²⁵²

APPENDIX A: CURVE VARIATIONAL THEORY

Here we sketch merely the derivation of Eqs. (16) and (17) because the derivation of Eq. (15) is trivial.

For convenience, we denote $\mathbf{e}_1 = \mathbf{N}$, $\mathbf{e}_2 = \mathbf{B}$, $\mathbf{e}_3 = \mathbf{T}$. Then we have $d\mathbf{r} = \omega_3 \mathbf{e}_3$ and $d\mathbf{e}_i = \omega_{ij} \mathbf{e}_j$ where

$$\omega_3 = ds, \omega_{12} = \tau\omega_3, \omega_{13} = -\kappa\omega_3, \omega_{23} = 0. \quad (\text{A1})$$

Following the spirit of Ref. 49, any infinitesimal deformation of a curve can be achieved by a displacement vector at each point on the curve as

$$\delta\mathbf{r} \equiv \mathbf{v} = \Omega_1 \mathbf{e}_1 + \Omega_2 \mathbf{e}_2 + \Omega_3 \mathbf{e}_3, \quad (\text{A2})$$

where δ can be understood a variational operator. The frame is also changed because of the deformation of the

curve, which is denoted as

$$\delta\mathbf{e}_i = \Omega_{ij} \mathbf{e}_j, \quad (i = 1, 2, 3), \quad (\text{A3})$$

where $\Omega_{ij} = -\Omega_{ji}$, ($i, j = 1, 2, 3$) corresponds to the rotation of the frame due to the deformation of the curve. From $\delta d\mathbf{r} = d\delta\mathbf{r}$, $\delta d\mathbf{e}_j = d\delta\mathbf{e}_j$, and $\delta d\phi = d\delta\phi = 0$, we can derive

$$\delta\omega_3 = \Omega_1\omega_{13} + \Omega_2\omega_{23} + d\Omega_3, \quad (\text{A4})$$

$$\omega_3\Omega_{31} = d\Omega_1 + \Omega_2\omega_{21} + \Omega_3\omega_{31}, \quad (\text{A5})$$

$$\omega_3\Omega_{32} = \Omega_1\omega_{12} + d\Omega_2 + \Omega_3\omega_{32}, \quad (\text{A6})$$

$$\delta\omega_{ij} = d\Omega_{ij} + \Omega_{il}\omega_{lj} - \omega_{il}\Omega_{lj}, \quad (\text{A7})$$

$$\delta\phi' ds = -\phi' \delta\omega_3. \quad (\text{A8})$$

Considering the above equations (A1), (A4)–(A8) and integral by parts as well as Stokes' theorem, we can derive Eqs. (16) and (17) from the free energy (14).

APPENDIX B: SURFACE VARIATIONAL THEORY

Following the spirit of Ref. 49, any infinitesimal deformation of a surface can be achieved by a displacement vector at each point on the surface as

$$\delta\mathbf{r} \equiv \mathbf{v} = \Omega_1 \mathbf{e}_1 + \Omega_2 \mathbf{e}_2 + \Omega_3 \mathbf{e}_3, \quad (\text{B1})$$

where δ can be understood a variational operator. The frame is also changed because of the deformation of the surface, which is still denoted as

$$\delta\mathbf{e}_i = \Omega_{ij} \mathbf{e}_j, \quad (i = 1, 2, 3), \quad (\text{B2})$$

where $\Omega_{ij} = -\Omega_{ji}$, ($i, j = 1, 2, 3$) corresponds to the rotation of the frame due to the deformation of the surface. From $\delta d\mathbf{r} = d\delta\mathbf{r}$, $\delta d\mathbf{e}_j = d\delta\mathbf{e}_j$, and Eqs. (2)–(5), we can derive

$$\delta\omega_1 = d\mathbf{v} \cdot \mathbf{e}_1 - \omega_2\Omega_{21}, \quad (\text{B3})$$

$$\delta\omega_2 = d\mathbf{v} \cdot \mathbf{e}_2 - \omega_1\Omega_{12}, \quad (\text{B4})$$

$$\Omega_{13} = \Omega_{3,1} + a\Omega_1 + b\Omega_2, \quad (\text{B5})$$

$$\Omega_{23} = \Omega_{3,2} + b\Omega_1 + c\Omega_2, \quad (\text{B6})$$

$$\delta\omega_{ij} = d\Omega_{ij} + \Omega_{il}\omega_{lj} - \omega_{il}\Omega_{lj}. \quad (\text{B7})$$

These equations are the essential equations of the surface variational theory based on the moving frame method. With them as well as Eqs. (5) and (6), we can easily derive

$$\delta dA = (\text{div } \mathbf{v} - 2H\Omega_3) dA, \quad (\text{B8})$$

$$\delta(2H) = [\nabla^2 + (4H^2 - 2K)]\Omega_3 + \nabla(2H) \cdot \mathbf{v}, \quad (\text{B9})$$

$$\delta K = \nabla \cdot \tilde{\nabla}\Omega_3 + 2KH\Omega_3 + \nabla K \cdot \mathbf{v}. \quad (\text{B10})$$

Using the above three equations and the Stokes' theorem, we can easily derive Eq. (57) from the free energy (56), or Eqs. (87)–(90) from the free energy (86), and so on.

APPENDIX C: STOKES' THEOREM AND THE OTHER IMPORTANT GEOMETRIC RELATIONS

The Stokes' theorem is a crucial theorem in differential geometry. Let us denote the boundary of domain \mathcal{D} as $\partial\mathcal{D}$. The Stokes' theorem states as: If ω is a differential form on $\partial\mathcal{D}$, then

$$\oint_{\partial\mathcal{D}} \omega = \int_{\mathcal{D}} d\omega. \quad (\text{C1})$$

In particular, $\int_{\mathcal{D}} d\omega = 0$ for a closed domain \mathcal{D} .

It contains a lot of geometric relations, which are listed as follows.

(i) For any smooth functions f and h on 2D domain \mathcal{D} , we have

$$\int_{\mathcal{D}} (fd*dh - hd*df) = \oint_{\partial\mathcal{D}} (f*dh - h*df), \quad (\text{C2})$$

$$\int_{\mathcal{D}} (fd*\tilde{d}h - hd*\tilde{d}f) = \oint_{\partial\mathcal{D}} (f*\tilde{d}h - h*\tilde{d}f), \quad (\text{C3})$$

$$\int_{\mathcal{D}} (fd*\tilde{d}h - hd*\tilde{d}f) = \oint_{\partial\mathcal{D}} (f*\tilde{d}h - h*\tilde{d}f). \quad (\text{C4})$$

where \tilde{d} and $*$ are generalized differential operator and Hodge star which satisfy $\tilde{d}f = f_1\omega_{13} + f_2\omega_{23}$ and $*\tilde{d}f = f_1\omega_{23} - f_2\omega_{13}$ if $df = f_1\omega_1 + f_2\omega_2$.⁴⁹

(ii) If \mathbf{u} is a vector defined on a closed surface, then

$$\int d\mathbf{u} \cdot \wedge * d\mathbf{u} = - \int \mathbf{u} \cdot d * d\mathbf{u}, \quad (\text{C5})$$

where the dot represents the inner product of vectors.

(iii) For the tensors \mathfrak{S} and \mathfrak{M} defined in Sec. II, we have

$$\oint_{\partial\mathcal{D}} \mathfrak{S} \cdot \mathbf{b} ds = \int_{\mathcal{D}} \text{div } \mathfrak{S} dA, \quad (\text{C6})$$

$$\oint_{\partial\mathcal{D}} \mathfrak{M} \cdot \mathbf{b} ds = \int_{\mathcal{D}} \text{div } \mathfrak{M} dA, \quad (\text{C7})$$

where \mathcal{D} is a 2D domain with boundary $\partial\mathcal{D}$ and \mathbf{b} is the normal vector of $\partial\mathcal{D}$ in the tangent plane.

The above three items are also called the Stokes' theorem in this review, which are widely used in the variational process.

The other geometric identities linking the vector form and differential form on a smooth surface used in this review are summarized as follows without additional proof.

$$(\text{curl } \mathbf{u}) dA = d(\mathbf{u} \cdot d\mathbf{r}), \quad (\text{C8})$$

$$(\text{div } \mathbf{u}) dA = d(*\mathbf{u} \cdot d\mathbf{r}), \quad (\text{C9})$$

$$(\tilde{\nabla} \cdot \mathbf{u}) dA = d(\tilde{*}\mathbf{u} \cdot \tilde{d}\mathbf{r}), \quad (\text{C10})$$

$$(\bar{\nabla} \cdot \mathbf{u}) dA = d(*\mathbf{u} \cdot \tilde{d}\mathbf{r}), \quad (\text{C11})$$

$$\nabla f \cdot d\mathbf{r} = df, \quad (\text{C12})$$

$$\tilde{\nabla} f \cdot d\mathbf{r} = \tilde{d}f, \quad (\text{C13})$$

$$(\nabla^2 f) dA = d * df, \quad (\text{C14})$$

$$(\nabla \cdot \bar{\nabla} f) dA = d * \tilde{d}f, \quad (\text{C15})$$

$$(\nabla \cdot \tilde{\nabla} f) dA = d\tilde{*}\tilde{d}f, \quad (\text{C16})$$

$$(\nabla f \cdot \mathbf{u}) dA = df \wedge *\mathbf{u} \cdot d\mathbf{r}, \quad (\text{C17})$$

$$(\nabla^2 \mathbf{u}) dA = d * d\mathbf{u}, \quad (\text{C18})$$

$$(\nabla \mathbf{u}) \cdot d\mathbf{r} = d\mathbf{u}. \quad (\text{C19})$$

* Electronic address: tuzc@bnu.edu.cn

† Electronic address: oy@itp.ac.cn

¹ L. A. Godoy, *Meccanica* 41, 529 (2006).

² A. E. H. Love, *A Treatise on the Mathematical Theory of Elasticity*, Dover, New York (1944).

³ L. D. Landau and E. M. Lifshitz, *Theory of Elasticity*, Butterworth-Heinemann, Oxford (1997).

⁴ J. M. Gere and S. P. Timoshenko, *Mechanics of Materials*, Chapman & Hall, London (1984).

⁵ F. Tanaka and H. Takahashi, *J. Chem. Phys.* 83, 6017 (1985).

⁶ W. Zhao, H. J. Zhou, and Z. C. Ou-Yang, *Phys. Rev. E* 58, 8040 (1998).

⁷ H. Zhou and Z. C. Ou-Yang, *Phys. Rev. E* 58, 4816 (1998).

⁸ H. Zhou and Z. C. Ou-Yang, *J. Chem. Phys.* 110, 1247 (1999).

⁹ B. Fain and J. Rudnick, *Phys. Rev. E* 60, 7239 (1999).

¹⁰ S. Panyukov and Y. Rabin, *Phys. Rev. E* 64, 011909 (2001).

¹¹ S. Zhang, X. Zuo, M. Xia, S. Zhao, and E. Zhang, *Phys. Rev. E* 70, 051902 (2004).

¹² S. Zhao, S. Zhang, Z. Yao, and L. Zhang, *Phys. Rev. E* 74, 032801 (2006).

¹³ B. Fain, J. Rudnick, and S. Östlund, *Phys. Rev. E* 55, 7364 (1997).

¹⁴ C. W. Wolgemuth and S. X. Sun, *Phys. Rev. Lett.* 97, 248101 (2006).

¹⁵ B. Smith, Y. V. Zastavker and G. B. Benedek, *Phys. Rev. Lett.* 87, 278101 (2001).

¹⁶ D. A. Kessler and Y. Rabin, *Phys. Rev. Lett.* 90, 024301 (2003).

¹⁷ Z. Zhou, *Mod. Phys. Lett. B* 19, 249 (2005).

¹⁸ Z. Zhou, P.-Y. Lai and B. Joós, *Phys. Rev. E* 71, 052801 (2005).

¹⁹ H. Wada and R. R. Netz, *Europhys. Lett.* 77, 68001 (2007).

²⁰ Q. H. Liu, Y. W. Jia, W. H. Qi, Z. C. Ou-Yang, *Phys. Lett. A* 317, 401 (2003).

²¹ Q. H. Liu, Y. F. Liu, B. Hu and Z. C. Ou-Yang, *Phys. Lett. A* 352, 358 (2006).

²² A. Goriely and M. Tabor, *Phys. Rev. Lett.* 80, 1564 (1998).

²³ A. Goriely and S. Neukirch, *Phys. Rev. Lett.* 97, 184302 (2006).

²⁴ R. E. Goldstein, A. Goriely, G. Huber and C. W. Wolgemuth, *Phys. Rev. Lett.* 84, 1631 (2000).

²⁵ J. Lidmar, L. Mirny and D. R. Nelson, *Phys. Rev. E* 68,

- 051910 (2003).
- ²⁶ T. T. Nguyen, R. F. Bruinsma, and W. M. Gelbart, *Phys. Rev. E* 72, 051923 (2005).
- ²⁷ W. S. Klug, R. F. Bruinsma, J. Michel, C. M. Knobler, I. L. Ivanovska, C. F. Schmidt, and G. J. L. Wuite, *Phys. Rev. Lett.* 97, 228101 (2006).
- ²⁸ P. B. Canham, *J. Theor. Biol.* 26, 61 (1970).
- ²⁹ W. Helfrich, *Z. Naturforsch. C* 28, 693 (1973).
- ³⁰ E. A. Evans, *Biophys. J.* 13, 941 (1973).
- ³¹ J. T. Jenkins, *SIAM J. Appl. Math.* 32, 755 (1977)
- ³² R. Lipowsky, *Nature* 349, 475 (1991).
- ³³ U. Seifert, *Adv. Phys.* 46, 13 (1997).
- ³⁴ Z. C. Ou-Yang, J. X. Liu and Y. Z. Xie, *Geometric Methods in the Elastic Theory of Membranes in Liquid Crystal Phases*, World Scientific, Singapore (1999).
- ³⁵ O. Y. Zhong-can, *Thin Solid Films* 393, 19 (2001).
- ³⁶ Z. C. Tu, *AAPPS Bulletin* 16, 30 (2006).
- ³⁷ X. Y. Kong and Z. L. Wang, *Nano Lett.* 3, 1625 (2003).
- ³⁸ W. L. Hughes and Z. L. Wang, *J. Am. Chem. Soc.* 126, 6703 (2004).
- ³⁹ Z. C. Tu, Q. X. Li and X. Hu, *Phys. Rev. B* 73, 115402 (2006).
- ⁴⁰ B. I. Yakobson, C. J. Brabec and J. Bernholc, *Phys. Rev. Lett.* 76, 2511 (1996).
- ⁴¹ J. P. Lu, *Phys. Rev. Lett.* 79, 1297 (1997).
- ⁴² O. Y. Zhongcan, Z. B. Su and C. L. Wang, *Phys. Rev. Lett.* 78, 4055 (1997).
- ⁴³ V. N. Popov, V. E. Van Doren and M. Balkanski, *Phys. Rev. B* 61, 3078 (2000).
- ⁴⁴ Z. C. Tu and Z. C. Ou-Yang, *Phys. Rev. B* 65, 233407 (2002).
- ⁴⁵ H. Rafii-Tabar, *Phys. Rep.* 390, 235 (2004).
- ⁴⁶ D. Qian, G. J. Wagner, W. K. Liu, M. Yu and R. S. Ruoff, *Appl. Mech. Rev.* 55, 495 (2002).
- ⁴⁷ M. Do Carmo, *Differential Geometry of Curves and Surfaces* (Prentice-Hall, 1976).
- ⁴⁸ S. S. Chern and W. H. Chern, *Lecture on Differential Geometry* (Beijing University Press, Beijing, 1983).
- ⁴⁹ Z. C. Tu and Z. C. Ou-Yang, *J. Phys. A: Math. Gen.* 37, 11407 (2004).
- ⁵⁰ T. McMillen and A. Goriely, *J. Nonlinear. Sci.* 12, 241 (2002).
- ⁵¹ A. Goriely and P. Shipman, *Phys. Rev. E* 61, 4508 (2000).
- ⁵² W. Helfrich, *Langmuir* 7, 567 (1991).
- ⁵³ J. Yan, R. Kawamura, and J. F. Marko, *Phys. Rev. E* 71, 061905 (2005).
- ⁵⁴ M. Sano, A. Kamino, J. Okamura, and S. Shinkai, *Science* 293, 1299 (2001).
- ⁵⁵ H. Yamakawa and W. H. Stockmayer, *J. Chem. Phys.* 57, 2843 (1972).
- ⁵⁶ J. L. Ericksen and C. Truesdell, *Arch. Rational Mech. Anal.* 1, 295 (1957).
- ⁵⁷ R. Capovilla and J. Guven, *J. Phys. A: Math. Gen.* 35, 6233 (2002).
- ⁵⁸ H. Naito, M. Okuda, and Z. C. Ou-Yang, *Phys. Rev. E* 52, 2095 (1995).
- ⁵⁹ M. Giaquinta and S. Hildebrandt, *Calculus of variations* (Springer, Berlin, 1996).
- ⁶⁰ S. Tek, *J. Math. Phys.* 48, 013505 (2007).
- ⁶¹ Q. Zhang and G. Xu, *Several Pairs of Differential Operators and Their Applications in Variational Calculus of a General Third Order Energy*, <http://www.cc.ac.cn/07reseachreport/0705.pdf> (2007).
- ⁶² N. Sødergaard, *J. Phys. A: Math. Theor.* 40, 5067 (2007).
- ⁶³ J. F. Marko and E. D. Siggia, *Macromolecules* 28, 8759 (1995).
- ⁶⁴ H. J. Zhou, Y. Zhang and Z. C. Ou-Yang, *Phys. Rev. Lett.* 82, 4560 (1999).
- ⁶⁵ W. Han, S. M. Lindsay, M. Dlakic, and R. E. Harrington, *Nature* 386, 563 (1997)
- ⁶⁶ W. Han, M. Dlakic, Y. Zhu, S. M. Lindsay, and R. E. Harrington, *Proc. Natl. Acad. Sci. USA* 94, 10565 (1997).
- ⁶⁷ T. E. Cloutier and J. Widom, *Mol. Cell* 14, 355 (2004).
- ⁶⁸ R. Goetz and R. Lipowsky, *J. Chem. Phys.* 108, 7397 (1998).
- ⁶⁹ R. Goetz, G. Gompper and R. Lipowsky, *Phys. Rev. Lett.* 82, 221 (1999).
- ⁷⁰ J. C. Shillcock and R. Lipowsky, *J. Phys.: Condens. Matter* 18 S1191 (2006).
- ⁷¹ H. Noguchi and G. Gompper, *Phys. Rev. E* 73, 021903 (2006).
- ⁷² S. Svetina and B. Zeks, *Biomed. Biochem. Acta* 42, 86 (1983).
- ⁷³ U. Seifert, K. Berndl and R. Lipowsky, *Phys. Rev. A* 44, 1182 (1991).
- ⁷⁴ L. Miao, U. Seifert, M. Wortis and H. Döbereiner, *Phys. Rev. E* 49, 5389 (1994).
- ⁷⁵ O. Y. Zhongcan and W. Helfrich, *Phys. Rev. Lett.* 59, 2486, (1987)
- ⁷⁶ O. Y. Zhongcan and W. Helfrich, *Phys. Rev. A* 39, 5280 (1989).
- ⁷⁷ Z. C. OuYang, *Phys. Rev. A* 41, 4517 (1990).
- ⁷⁸ U. Seifert, *Phys. Rev. Lett.* 66, 2404 (1991).
- ⁷⁹ H. Naito, M. Okuda, and Z. C. Ou-Yang, *Phys. Rev. E* 48, 2304 (1993).
- ⁸⁰ M. Mutz and D. Bensimon, *Phys. Rev. A* 43, 4525 (1991).
- ⁸¹ J. G. Hu and Z. C. Ou-Yang, *Phys. Rev. E* 47, 461 (1993).
- ⁸² W. M. Zheng and J. Liu, *Phys. Rev. E* 48, 2856 (1993).
- ⁸³ T. Xu and Z. C. Ou-Yang, *Euro. Phys. J. E* 15, 9 (2004).
- ⁸⁴ R. Capovilla, J. Guven and E. Rojas, *J. Phys. A: Math. Gen.* 38, 8201 (2005)
- ⁸⁵ R. Capovilla, J. Guven and E. Rojas, *J. Phys. A: Math. Gen.* 38, 8841 (2005).
- ⁸⁶ Q. H. Liu, H. J. Zhou, J.-X. Liu and O. Zhong-Can, *Phys. Rev. E* 60, 3227 (1999).
- ⁸⁷ S. G. Zhang and Z. C. Ou-Yang, *Phys. Rev. E* 53, 4206 (1996).
- ⁸⁸ I. M. Mladenov, *Eur. Phys. J. B* 29, 327 (2002).
- ⁸⁹ G. Landolfi, *J. Phys. A: Math. Gen.* 36, 11937 (2003).
- ⁹⁰ K. Brakke, *Exp. Math.* 1, 141 (1992).
- ⁹¹ J. Yan, Q. H. Liu, J. X. Liu and Z. C. Ou-Yang, *Phys. Rev. E* 58, 4730 (1998).
- ⁹² J. J. Zhou, Y. Zhang, X. Zhou, Z. C. Ou-Yang, *Int. J. Mod. Phys. B* 15, 2977 (2001).
- ⁹³ Y. Zhang, X. Zhou, J. J. Zhou and Z. C. Ou-Yang, *Int. J. Mod. Phys. B* 16, 511 (2002).
- ⁹⁴ X. H. Zhou and S. G. Zhang, *Acta Phys. Sin.* 55, 5568 (2006).
- ⁹⁵ Q. Du, C. Liu, and X. Wang, *J. Comput. Phys.* 198, 450 (2004).
- ⁹⁶ Q. Du, C. Liu, and X. Wang, *J. Comput. Phys.* 212, 757 (2005)
- ⁹⁷ Q. Du, C. Liu, R. Ryham, X. Wang, *Comm. Pure Appl. Anal.* 4, 537 (2005).
- ⁹⁸ Q. Du, C. Liu and X. Wang, *J. Comput. Phys.* 212, 757 (2006).
- ⁹⁹ F. Feng and W. S. Klug, *J. Comput. Phys.* 220, 394 (2006).

- ¹⁰⁰ R. Capovilla and J. Guven, *J. Phys. A: Math. Gen.* 37, 5983 (2004).
- ¹⁰¹ A. Saitoh, K. Takiguchi, Y. Tanaka, and H. Hotani, *Proc. Natl. Acad. Sci.* 95, 1026 (1998).
- ¹⁰² F. Nomura, M. Nagata, T. Inaba, H. Hiramatsu, H. Hotani, and K. Takiguchi, *Proc. Natl. Acad. Sci.* 98, 2340 (2001).
- ¹⁰³ R. Capovilla, J. Guven and J. A. Santiago, *Phys. Rev. E* 66, 021607 (2002).
- ¹⁰⁴ S. S. Chern, *moving frame method* (talk, 2001).
- ¹⁰⁵ Z. C. Tu and Z. C. Ou-Yang, *Phys. Rev. E* 68, 061915 (2003).
- ¹⁰⁶ T. Umeda, Y. Suezaki, K. Takiguchi and H. Hotani, *Phys. Rev. E* 71, 011913 (2005).
- ¹⁰⁷ X. Wang and Q. Du, *J. Math. Biol.* 56, 347 (2008).
- ¹⁰⁸ M. Kaga and T. Ohta, *Eur. Phys. J. E* 21, 91 (2006).
- ¹⁰⁹ F. Jülicher and R. Lipowsky, *Phys. Rev. E* 53, 2670 (1996).
- ¹¹⁰ R. Lipowsky and R. Dimova, *J. Phys. Condens. Matter* 15, S31 (2003).
- ¹¹¹ T. Baumgart, S.T. Hess, and W. W. Webb, *Nature* 425, 821 (2003).
- ¹¹² T. Baumgart, S. Das, W. W. Webb, and J. T. Jenkins, *Biophys. J.* 89, 1067 (2005).
- ¹¹³ Z. C. Tu, L. Q. Ge, and Z. C. Ou-Yang, *Thin Solid Films* 509, 58 (2006).
- ¹¹⁴ K. Simons and E. Ikonen, *Nature* 387, 569 (1997).
- ¹¹⁵ Z. C. Tu and U. Seifert, *Phys. Rev. E* 76, 031603 (2007).
- ¹¹⁶ E. Sackmann and R. F. Bruinsma, *ChemPhysChem* 3, 262 (2002).
- ¹¹⁷ U. Seifert and R. Lipowsky, *Phys. Rev. A* 42, 4768 (1990).
- ¹¹⁸ D. Ni, H. Shi and Y. Yin, *Colloids and Surfaces B* 46, 162 (2005).
- ¹¹⁹ D. Ni, H. Shi and Y. Yin, *Int. J. Mod. Phys. B* 20, 1201 (2006).
- ¹²⁰ R. Capovilla and J. Guven, *Phys. Rev. E* 66, 041604 (2002).
- ¹²¹ M. Deserno, M. M. Müller and J. Guven, *Phys. Rev. E* 76, 011605 (2007).
- ¹²² P. Zihlerl and S. Svetina, *Proc. Natl. Acad. Sci. USA* 104, 761 (2007).
- ¹²³ P. Graf, R. Finken and U. Seifert, *Langmuir* 22, 7117 (2006).
- ¹²⁴ W. Rawicz, K. C. Olbrich, T. McIntosh, D. Needham, and E. Evans, *Biophys. J.* 79, 328 (2000).
- ¹²⁵ S. J. Singer and G. L. Nicolson, *Science* 175, 720 (1972).
- ¹²⁶ E. A. Evans, R. Waugh and L. Melnik, *Biophys. J.* 16, 585 (1976).
- ¹²⁷ E. A. Evans, *Biophys. J.* 43, 27 (1983).
- ¹²⁸ H. Engelhardt and E. Sackmann, *Biophys. J.* 54, 495 (1988).
- ¹²⁹ G. Lenormand, S. Hénon, A. Richert, J. Siméon, and F. Gallet *Biophys. J.* 81, 43 (2001).
- ¹³⁰ Y. C. Fung and P. Tong, *Biophys. J.* 8, 175 (1968).
- ¹³¹ E. A. Evans, *Biophys. J.* 13, 926 (1973).
- ¹³² D. H. Boal, U. Seifert and A. Zilker, *Phys. Rev. Lett.* 69, 3405 (1992).
- ¹³³ E. Sackmann, A. R. Bausch and L. Vonna, *Physics of Composite Cell Membrane and Actin Based Cytoskeleton*, in *Physics of bio-molecules and cells*, Edited by H. Flyvbjerg, F. Jülicher, P. Ormos And F. David, (Springer, Berlin, 2002).
- ¹³⁴ J. F. Nye, *Physical Properties of Crystals* (Clarendon Press, Oxford, 1985)
- ¹³⁵ \tilde{k} in this review is twice of the traditional convention of the shear modulus.
- ¹³⁶ C. V. Westenholtz, *Differential Forms in Mathematical Physics* (North-Holland, Amsterdam, 1981).
- ¹³⁷ Z. C. Tu, L. Q. Ge, J. B. Li, and Z. C. Ou-Yang, *Phys. Rev. E* 72, 021806 (2005).
- ¹³⁸ A. V. Pogorelov, *Bendings of surfaces and stability of shells* (American Mathematical Society, Providence, 1980).
- ¹³⁹ A. K. Geim and K. S. Novoselov, *Nature Mater.* 6, 183 (2007).
- ¹⁴⁰ K. S. Novoselov, A. K. Geim, S. V. Morozov, D. Jiang, Y. Zhang, S. V. Dubonos, I. V. Grigorieva and A. A. Firsov, *Science* 306, 666 (2004).
- ¹⁴¹ K. S. Novoselov, D. Jiang, F. Schedin, T. J. Booth, V. V. Khotkevich, S. V. Morozov and A. K. Geim, *Proc. Natl. Acad. Sci. USA* 102, 10451 (2005).
- ¹⁴² N. D. Mermin, *Phys. Rev.* 176, 250 (1968).
- ¹⁴³ J. C. Meyer, A. K. Geim, M. I. Katsnelson, K. S. Novoselov, T. J. Booth and S. Roth, *Nature* 446, 60 (2007).
- ¹⁴⁴ A. Fasolino, J. H. Los and M. I. Katsnelson, *Nature Mater.* 6, 858 (2007).
- ¹⁴⁵ N. García, arxiv: cond-mat/0703515.
- ¹⁴⁶ T. Lenosky, X. Gonze, M. Teter, and V. Elser, *Nature* 355, 333 (1992).
- ¹⁴⁷ X. Zhou, H. Chen, J. J. Zhou, and Z. C. Ou-Yang, *Physica B* 304, 86 (2001).
- ¹⁴⁸ R. Nicklow, N. Wakabayashi, and H. G. Smith, *Phys. Rev. B* 5, 4951 (1972).
- ¹⁴⁹ X. Gonze, J. M. Beuken, R. Caracas, F. Detraux, M. Fuchs, G. M. Rignanese, L. Sindic, M. Verstraete, G. Zerah, F. Jollet, M. Torrent, A. Roy, M. Mikami, Ph. Ghosez, J. Y. Raty, and D. C. Allan, *Comput. Mater. Sci.* 25, 478 (2002).
- ¹⁵⁰ N. Troullier and J. L. Martins, *Phys. Rev. B* 43, 1993 (1991).
- ¹⁵¹ H. J. Monkhorst and J. D. Pack, *Phys. Rev. B* 13, 5188 (1976).
- ¹⁵² D. M. Ceperley and B. J. Alder, *Phys. Rev. Lett.* 45, 566 (1980).
- ¹⁵³ J. P. Perdew and Y. Wang, *Phys. Rev. B* 45, 13244 (1992).
- ¹⁵⁴ Z. C. Tu and Z. C. Ou-Yang, *J. Comput. Theor. Nanosci.* 3, 375 (2006).
- ¹⁵⁵ K. Komatsu, *J. Phys. Soc. Jpn.* 10, 346 (1955).
- ¹⁵⁶ K. Komatsu, *J. Phys. Chem. Solids* 6, 380 (1958).
- ¹⁵⁷ T. Nihira and T. Iwata, *Phys. Rev. B* 68, 134305 (2003).
- ¹⁵⁸ O. L. Blakeslee, D. G. Proctor, E. J. Seldin, G. B. Spence, and T. Weng, *J. Appl. Phys.* 41, 3373 (1970).
- ¹⁵⁹ A. H. Neto and E. A. Kim, arXiv:cond-mat/0702562.
- ¹⁶⁰ S. Iijima, *Nature* 354, 56 (1991).
- ¹⁶¹ S. Iijima and T. Ichihashi, *Nature* 363, 603 (1993).
- ¹⁶² R. Saito, M. S. Dresselhaus, and G. Dresselhaus, *Physical Properties of Carbon Nanotubes* (Imperial College Press, London, 1998).
- ¹⁶³ J. W. Mintmire, B. I. Dunlap C. T. White, *Phys. Rev. Lett.* 68, 631 (1992).
- ¹⁶⁴ A. Krishnan, E. Dujardin, T. W. Ebbesen, P. N. Yianilos, and M. M. J. Treacy, *Phys. Rev. B* 58, 14013 (1998).
- ¹⁶⁵ M. M. J. Treacy, T. W. Ebbesen, and J. M. Gibson, *Nature* 381, 678 (1996).
- ¹⁶⁶ E. W. Wong, P. E. Sheehan, and C. M. Lieber, *Science* 277, 1971 (1997).
- ¹⁶⁷ K. N. Kudin, G. E. Scuseria, and B. I. Yakobson, *Phys.*

- Rev. B* 64, 235406 (2001).
- 168 X. Zhou, J. Zhou and Z. C. Ou-Yang, *Phys. Rev. B* 62, 13692 (2000).
- 169 T. Vodenitcharova and L. C. Zhang, *Phys. Rev. B* 68, 165401 (2003).
- 170 A. Pantano, M. C. Boyce and D. M. Parks, *Phys. Rev. Lett.* 91, 145504 (2003).
- 171 A. Pantano, D. M. Parks and M. C. Boyce, *J. Mech. Phys. Solids* 52, 789 (2004).
- 172 X. Chen and G. Cao, *Nanotechnology* 17, 1004 (2006).
- 173 L. Wang, Q. Zheng, J. Z. Liu and Q. Jiang, *Phys. Rev. Lett.* 95, 105501 (2005).
- 174 A. Sears and R. C. Batra, *Phys. Rev. B* 69, 235406 (2004).
- 175 K. I. Tserpes and P. Papanikos, *Composites: Part B* 36, 468 (2005).
- 176 E. Hernandez, C. Goze, P. Bernier, and A. Rubio, *Appl. Phys. A: Solids Surf.* 68, 287 (1999).
- 177 L. Shen and J. Li, *Phys. Rev. B* 71, 165427 (2005).
- 178 C. Li and T. Chou, *Int. J. Solids Struct.* 40, 2487 (2003).
- 179 W. X. Bao, C. C. Zhu, W. Z. Cui, *Physica B* 352, 156 (2004).
- 180 G. Zhou, W. Duan, and B. Gu, *Chem. Phys. Lett.* 333, 344 (2001).
- 181 Y. Huang, J. Wu and K. C. Hwang, *Phys. Rev. B* 74, 245413 (2006).
- 182 T. Chang and H. Gao, *J. Mech. Phys. Solids* 51, 1059 (2003).
- 183 C. Li and T. Chou, *Phys. Rev. B* 69, 073401 (2004).
- 184 T. Chang, J. Geng and X. Guo, *Appl. Phys. Lett.* 87, 251929 (2005).
- 185 H. Mori, Y. Hirai, S. Ogata, S. Akita and Y. Nakayama, *Jpn. J. Appl. Phys.* 44, L1307 (2005).
- 186 S. Govindjee and J. L. Sackman, *Solid State Commun.* 110, 227 (1999).
- 187 P. Liu, Y. W. Zhang, C. Lu and K. Y. Lam, *J. Phys. D* 37, 2358 (2004).
- 188 B. Liu, Y. Huang, H. Jiang, S. Qu and K. C. Hwang, *Comput. Methods Appl. Mech. Engrg.* 193, 1849 (2004).
- 189 X. Guo, A. Y. T. Leung, H. Jiang, X. Q. He, and Y. Huang, *J. Appl. Mech.* 74, 347 (2007).
- 190 C. M. Wang, Y. Q. Ma, Y. Y. Zhang and K. K. Ang, *J. Appl. Phys.* 99, 114317 (2006).
- 191 V. M. Harik, *Comput. Mater. Sci.* 24, 328 (2002).
- 192 K. M. Liew, C. H. Wong, X. Q. He, M. J. Tan and S. A. Meguid, *Phys. Rev. B* 69, 115429 (2004).
- 193 A. Sears and R. C. Batra, *Phys. Rev. B* 73, 085410 (2006).
- 194 G. Cao and X. Chen, *Nanotechnology* 17, 3844 (2006).
- 195 Q. Wang and V. K. Varadan, *Smart Mater. Struct.* 14, 281 (2005).
- 196 Y. Y. Zhang, C. M. Wang and V. B. C. Tan, *J. Engin. Mech.* 132, 952 (2006).
- 197 C. Q. Ru, *Phys. Rev. B* 62, 9973 (2000).
- 198 P. S. Das and L.T. Wille, *Comput. Mater. Sci.* 24, 159 (2002).
- 199 T. Xiao, X. Xu and K. Liao, *J. Appl. Phys.* 95, 8145 (2004).
- 200 X. Q. He, S. Kitipornchai and K. M. Liew, *J. Mech. Phys. Solids* 53, 303 (2005).
- 201 J. F. Waters, L. Riestler and M. Jouzi, P. R. Guduru and J. M. Xu, *Appl. Phys. Lett.* 85, 1787 (2004).
- 202 J. F. Waters, P. R. Guduru and J. M. Xu, *Composites Sci. Technol.* 66, 1141 (2006).
- 203 M. Hasegawa and K. Nishidate, *Phys. Rev. B* 74, 115401 (2006).
- 204 I. Palaci, S. Fedrigo, H. Brune, C. Klinke, M. Chen and E. Riedo, *Phys. Rev. Lett.* 94, 175502 (2005).
- 205 X. B. Dai, H. Merlitz, and C. X. Wu, *Eur. Phys. J. B* 54, 109 (2006).
- 206 G. Cao and X. Chen, *Phys. Rev. B* 73, 155435 (2006).
- 207 T. Chang, W. Guo and X. Guo, *Phys. Rev. B* 72, 064101 (2005).
- 208 Q. Wang, T. Hu, G. Chen and Q. Jiang, *Phys. Rev. B* 71, 045403 (2005).
- 209 X. Wang and H. K. Yang, *Phys. Rev. B* 73, 085409 (2006).
- 210 C. Q. Ru, *J. Mech. Phys. Solids* 49, 1265 (2001).
- 211 S. Kitipornchai, X. Q. He and K. M. Liew, *J. Appl. Phys.* 97, 114318 (2005).
- 212 Y. Q. Zhang, G. R. Liu, H. F. Qiang and G. Y. Li, *Int. J. Mech. Sci.* 48, 53 (2006).
- 213 H. K. Yang and X. Wang, *Modelling Simul. Mater. Sci. Eng.* 14, 99 (2006).
- 214 X. Wang, G. Lu and Y. J. Lu, *Int. J. Solids Struct.* 44, 336 (2007).
- 215 Q. Han and G. Lu, *Eur. J. Mech. A* 22, 875 (2003).
- 216 H. Shen, *Int. J. Solids Struct.* 41, 2643 (2004).
- 217 H. Shen and C. Zhang, *Phys. Rev. B* 74, 035410 (2006).
- 218 A. Y. T. Leung, X. Guo, X. Q. He, H. Jiang and Y. Huang, *J. Appl. Phys.* 99, 124308 (2006).
- 219 X. Yao and Q. Han, *Eur. J. Mech. A* 26, 20 (2007).
- 220 X. Y. Wang and X. Wang, *Composites: Part B* 35, 79 (2004).
- 221 P. Zhang, P. E. Lammert and V. H. Crespi, *Phys. Rev. Lett.* 81, 5346 (1998).
- 222 D. Srivastava, M. Menon and K. Cho, *Phys. Rev. Lett.* 83, 2973 (1999).
- 223 D. Hui, M. Chipara, J. Sankar and K. T. Lau, *J. Comput. Theor. Nanosci.* 1, 209 (2004).
- 224 K. T. Lau, M. Chipara, H. Y. Ling and D. Hui, *Composites: Part B* 35, 95 (2004).
- 225 K. T. Lau, C. Gu and D. Hui, *Composites: Part B* 37, 425 (2006).
- 226 H. R. Lusti and A. A. Gusev, *Modelling Simul. Mater. Sci. Eng.* 12 S107 (2004).
- 227 T. Vodenitcharova and L. C. Zhang, *Int. J. Solids Struct.* 43, 3006 (2006).
- 228 J. Varghese and J. Whitcomb, *Mech. Adv. Mater. Struct.* 13, 227 (2006).
- 229 S. Rajendran and C. D. Reddy, *J. Comput. Theor. Nanosci.* 3, 382 (2006).
- 230 D. Sánchez-Portal, E. Artacho, J. M. Soler, A. Rubio, and P. Ordejón, *Phys. Rev. B* 59, 12678 (1999).
- 231 M. Arroyo and T. Belytschko, *Phys. Rev. B* 69, 115415 (2004).
- 232 P. Zhang, Y. Huang, P. H. Geubelle, P. A. Klein, and K. C. Hwang, *Int. J. Solids Struct.* 39, 3893 (2002).
- 233 D. Caillerie, A. Mourad and A. Raoult, *J. Elasticity* 84, 33 (2006).
- 234 Q. Wang, *Int. J. Solids Struct.* 41, 5451 (2004).
- 235 N. Chandra, S. Namilae and C. Shet, *Phys. Rev. B* 69, 094101 (2004).
- 236 Q. Lu and B. Bhattacharya, *Nanotechnology* 16, 555 (2005).
- 237 Y. Yin, H.-Y. Yeh and J. Yin. *IEEE Proc.-Nanobiotechnol.* 153, 7 (2006).
- 238 S. K. Boey, D. H. Boal and D. E. Discher, *Biophys. J.* 75, 1573 (1998).
- 239 D. E. Discher, D. H. Boal, and S. K. Boey, *Biophys. J.* 75, 1584 (1998).

- ²⁴⁰ G. Lim, M. Wortis, and R. Mukhopadhyay, *Proc. Natl. Acad. Sci. USA* 99, 16766 (2002).
- ²⁴¹ M. Kraus, W. Wintz, U. Seifert and R. Lipowsky, *Phys. Rev. Lett.* 77, 3685 (1996).
- ²⁴² R. Finken and U. Seifert, *J. Phys.: Condens. Matter* 18, L185 (2006).
- ²⁴³ H. Noguchi and G. Gompper, *Proc. Natl. Acad. Sci. USA* 102, 14159 (2005).
- ²⁴⁴ C. Misbah, *Phys. Rev. Lett.* 96, 028104 (2006).
- ²⁴⁵ J. M. Skotheim and T. W. Secomb, *Phys. Rev. Lett.* 98, 078301 (2007).
- ²⁴⁶ X. Wang and H. L. Dai, *Carbon* 44, 158 (2006).
- ²⁴⁷ V. R. Coluci, S. O. Dantas, A. Jorio, and D. S. Galvão, *Phys. Rev. B* 75, 075417 (2007).
- ²⁴⁸ A. F. da Fonseca and D. S. Galvão, *Phys. Rev. Lett.* 92, 175502 (2004).
- ²⁴⁹ A. F. da Fonseca, C. P. Malta, and D. S. Galvão, *J. Appl. Phys.* 99, 094310 (2006).
- ²⁵⁰ M. Arroyo and T. Belytschko, *Phys. Rev. Lett.* 91, 215505 (2003).
- ²⁵¹ M. Arroyo and T. Belytschko, *Int. J. Numer. Meth. Engng.* 59, 419 (2004).
- ²⁵² Z. Zhang, H. T. Davis, and D. M. Kroll, *Phys. Rev. E* 48, R651 (1993).